Ore Geology Reviews 104 (2019) 46–71

Contents lists available at ScienceDirect

Ore Geology Reviews

journal homepage: www.elsevier.com/locate/oregeorev

Carbonate-related metallic and non-metallic mineralization within and proximal to granites (Fichtelgebirge Pluton, Germany): "Mantle-crust marker mineralization"

H.G. Dill[a,*], J. Kolb[b]

[a] Gottfried Wilhelm Leibniz University, Welfengarten 1, D-30167 Hannover, Germany
[b] Karlsruhe Institute of Technology, Institute of Applied Geosciences, Geochemistry and Economic Geology Group, Adenauerring 20b, D-76131 Karlsruhe, Germany

ARTICLE INFO

Keywords:
Carbonate-related mineralization
Granite suite
Mantle-crust marker mineralization
Fichtelgebirge Pluton, Germany

ABSTRACT

Metacarbonate rocks (marble, calcsilicate rock, skarn) hosting strata- and structurebound Fe-, As-Sb, Bi-, Ni-Co, Cu-Pb-Zn, U-, W- ore minerals as well as talc, clay minerals, barite and fluorite are widespread in the country rocks south of the collisional calc-alkaline felsic to intermediate intrusive rocks of the Fichtelgebirge Pluton, Germany. At its western rim, thrustbound and vein-type mineral assemblages with Au-As-Sb and F-Ba minerals associated with carbonate gangue minerals developed. Only recently, a calcite-hosted Sb mineralization was encountered in a deep-seated lineamentary fault zone cutting through metaultrabasic rocks along the northern edge of the granites. The same structure zone forms the loci of calcite-bearing U episyenite situated within this pluton. A composite geological, mineralogical and chemical (major and trace elements, REE, C- and O isotopes) study has been conducted to distinguish the heat and element source in subcrustal or deep-seated crustal areas and in the largely exposed granite complex. Only Sn-W skarn deposits are genetically related to the highly fractionated granitic members of the Variscan pluton. Pegmatite skarn has a strong subcrustal component as to the heat source and the provenance of rare elements and a moderate crustal one as far as the silicates are concerned. Deep-seated fault zones were active over a rather long period of time and acted as conduits venting magmas and hydrothermal fluids from the waning stages of the Variscan deformation through the Neogene. Calcsilicate and carbonate mineral assemblages are an efficacious tool to constrain the physico-chemical regime in this mineral province, covering the temperature range from 745 °C down to 53 °C in a medium to low pressure regime at strongly varying redox conditions. The major and trace elements, the REE variation, the Ce and Eu anomalies as well as carbon and oxygen isotopes of the various mineral assemblages enable us to identify the fluid sources and depict the element concentration processes, e.g., mixing of fluids, connate fluid and meteoric fluid interaction. From the economic point of view, the mineralizing system is most prospective for rare element deposits, talc, kaolinite-group minerals, iron, and uranium. Accumulations of fluorite and barite are sub-economic in mineral assemblages inside as well as outside the granites, while base metals and precious metals are only of mineralogical interest.

1. Introduction

There are numerous studies of granite-hosted and granite-related ore deposits of Sn, W and U or granitic pegmatites enriched in rare metals such as Li, Be, Nb, Ta and gemstones like topaz, aquamarine and colorful tourmaline. Any attempt to list these publications, even if it includes only part of the above commodities, would seriously fall short of completeness and only a sequence of comprehensive studies on economic geology, where this issue is addressed, are presented here, instead (Gilbert et al., 2007; Ridley, 2013; Dill, 2010, 2015a,b). Considering the concentration of W, Fe and base metals, calcareous rocks are held to play a prominent role in the close proximity to granites, where they lead to skarn deposits (Timon Sanchez et al., 2009; Song et al., 2014). In the current study, we focus on ore mineral assemblages containing, e.g., Sb, As, Hg, W, U as well as concentrations of industrial minerals such as talc, barite and fluorite, all of which are intergrown with calcite, dolomite or siderite forming the major gangue minerals (Table 1). There are also many hydrothermal-metasomatic Fe-

* Corresponding author.
E-mail address: haralddill@web.de (H.G. Dill).
URL: http://hgeodill.de (H.G. Dill).

https://doi.org/10.1016/j.oregeorev.2018.10.011
Received 7 June 2018; Received in revised form 10 October 2018; Accepted 19 October 2018
Available online 21 October 2018
0169-1368/

Table 1
Carbonate-hosted mineral deposits, their country rocks and mineral assemblages and the environment of formation of carbonate mineralization (REE, isotopes, mineralogy etc.) For locality, see Fig. 1b.

Site (number refers to Fig. 1c)	Country rocks	Carbonate minerals	Au-As-Bi minerals	Hg-Sb-Mo minerals	Cu-Pb-Zn-Ag minerals	Ni-Co minerals	U-W minerals	Ba-F minerals	Hydro-silicates	Ca-Mg-Fe-Be silicates	Environment of formation of carbonate mineralization (REE, isotopes, mineralogy etc.)
1 Brandholz-Goldkronach	Metabasalt keratophyre phyllite slate	Dolomite ankerite siderite rhodochrosite	**Native gold** arsenopyrite Bi-sulfide	***Stibnite*** Sb-sulfosalts native Sb Mo-sulfide	Ag-Cu fahlore	---	Scheelite Wolframite	Barite	Kaolinite chlorite muscovite	Stilbite	Eh varying: Eh < 0 to (Eh > 0), connate fluid interaction, younger than the massive dolomitization of the Wundsiedel Marble at Göpfersgrün, moderate subcrustal physical-chemical impact
2.Warmen-steinach (Mittelberg, Schanzberg)	Quartz-phyllite orthogneiss	***Ankerite*** ferro-dolomite ***siderite*** calcite	---	---	Cu sulfide	---	---	***Barite fluorite***	---		Fluorite: alkaline fluids gneissic leachate, Eh varying Eh > 0 (Eh <0), connate fluid interaction, moderate subcrustal physical-chemical impact
3. Holenbrunn	**Marble**	Calcite dolomite siderite	Arsenopyrite	Sb-sulfosalts Mo-sulfide	Cu-Pb-Zn-Ag sulfide	Pentlandite	---	Fluorite	Smectite vermiculite	Prehnite tremolite s.s.s. sphene clinozoisite-epidote s.s.s diopside	Carbonate: marine carbonate, hydrothermal overprint, Eh >0 , mixing of two hydrothermal fluids
4. Sinatengrün	**Marble,** skarn	Calcite Dolomite Ankerite Mn-siderite strontianite	---	Stibnite Sb-sulfosalts Hg-As tetrahedrite Mo-sulfide	Cu-Pb-Zn-Ag sulfide	Pyrrhotite	Scheelite	Fluorite	Talc chlorite muscovite smectite	Tremolite s.s.s. sphene clinozoisite-epidote s.s.s diopside vesuvianite	Carbonate: marine carbonate, hydrothermal overprint, Eh >>0, mixing of two hydrothermal fluids, fluids typical of MVT deposits and connate water/ meteoric water interaction, topomineralic F-mineralization
5. Göpfersgrün	Marble skarn	Dolomite calcite siderite (magnesite)	Bi-sulfide	Stibnite	Cu-sulfide	Pyrrhotite	Scheelite	Barite (fluorite)	***Talc*** chlorite corrensite vermiculite (kaolinite, nontronite)	Beryl tremolite s.s.s. clinozoisite-epidote s.s.s. vesuvianite grossular	Carbonate: marine carbonate, hydrothermal overprint, Eh strongly varying, Eh>> 0 to Eh <0, mixing of hydrothermal fluids resembling most closely those of skarn deposits the least subcrustal impact topomineralic F mineralization.
6. Thiersheim I	Marble	Dolomite, calcite ***Mn-siderite***	---	---	Cu-sulfide	---	---	---	Chlorite talc		Carbonate: marine carbonate, hydrothermal overprint, Eh < 0, mixing of hydrothermal fluids resembling most closely those of skarn deposits
7. Thiersheim II	Amphibolite-Gneiss	---	---	---	---	---	---	---	**Halloysite** (REE rich)		Eh << 0, pH << 7
8.Stemmas	**Marble**	Calcite siderite	Arsenopyrite	Mo-sulfide	Cu-Pb-Zn sulfide	Pyrrhotite	---	---	---	Tremolite s.s.s. vesuvianite grossular	Marine carbonate
9. Arzberg	Marble	**Siderite ankerite** dolomite calcite rhodochrosite	Arsenopyrite	---	Cu-Pb-Zn sulfide	Pyrrhotite	---	---	---	Tremolite s.s.s.	Marine carbonate, moderate subcrustal physical-chemical impact
10. Aign	Phyllite	**Siderite**	---	---	Cu-sulfide	---	---	---	---		
11. Neusorg	Marble	**Siderite** calcite	---	---	Cu-Pb-Zn sulfide	Pyrrhotite pyrite bravoite Ni-Co arsenide	---	---	muscovite		Carbonate: marine carbonate, with moderate hydrothermal overprint, primary features of the original limestone are well preserved,

(*continued on next page*)

Table 1 (*continued*)

											alkaline fluids, topo-mineralic re-deposition, Eh < 0, moderate subcrustal physical-chemical impact
12. Pullenreuth-Dechantsees-Kalkhaus Schindeloh	Marble with gneiss contact	**Siderite,** calcite	---	---	Cu-sulfide	Pyrrhotite	---	Fluorite	Muscovite phlogopite (talc)	Tremolite s.s.s. sphene	F: acidic fluids, gneissic leachate (altered), moderate subcrustal physico-chemical impact, topomineralic F mineralization
13. Tröstau	Calcsilicate rocks	**Siderite** ankerite calcite rhodochrosite	---	---	Zn-sulfide	---	---	---	---	Tremolite s.s.s. sphene grossular	Parent rocks: calcareous arenites, moderate subcrustal physico-chemical impact
14. Wurlitz	**Peridotite serpentinite**	Calcite dolomite	---	Stibnite	Cu-sulfide	Pyrrhotite pentlandite millerite	---	---	Stilpnome-lane chlorite vermiculite serpentine (talc)	Prehnite actinolite s.s.s clinozoisite-epidote s.s.s. vesuvianite grossular diopside	Eh varying: Eh < 0 to (Eh > 0), mixing of hydrothermal fluids similar to those from Göpfersgrün and Sinatengrün yet with no affiliation to skarn deposits
15. Hebanz	Granite-episyenite	Calcite, (dolomite)	---	---	---	---	**Uraninite**	---	Muscovite chlorite		Eh < 0, strong subcrustal physico-chemical impact
16. Gross-schloppen	Granite-(episyenite)	(calcite dolomite)	Bi-selenide (?)	---	Cu-Pb sulfide+ selenide	---	**Uraninite coffinite**	Fluorite barite	Muscovite chlorite kaolinite		Eh < 0, strong subcrustal physico-chemical impact
17. Lengenfeld	Granite-episyenite	Calcite (siderite)	---	---	---	---	**Brannerite decomp. to U leucoxene**	---	Muscovite chlorite		Eh < 0, strong subcrustal physico-chemical impact

Bold faced / italics = main ore mineral or rock targeted upon during mining or exploration; s.s.s. = solid solution series

Zonation

Carbonate-bearing vein-type deposits	Exocontact of granite
Carbonate-hosted mineral deposit (marginal facies relative to the Central Fichtelgebirge Lineament)	Exocontact of granite
Carbonate-hosted mineral deposit (central facies relative to the Central Fichtelgebirge Lineament)	Exocontact of granite
Non-carbonate-/ silicate hosted deposits (source rock of Ca-Mg)	Exocontact of granite
Episyenite (marginal facies relative to the Central Fichtelgebirge Lineament)	Endocontact of granite

replacement deposits that occur in limestone with ankerite and siderite as the principal ore, which is accompanied, in places, by base metal sulfides, hematite or barite (Ebner et al., 2000; Castorina and Masi, 2008; Dill et al., 2010; Huang et al., 2015). Some are genetically connected with granites close by, whereas others are interpreted in a different way excluding any granitic impact on their mineral association. The Fichtelgebirge Pluton is unrivaled as to the coverage with carbonate-hosted mineralization and it is located within a Central European region well studied as to its economic geology, as shown by the most recent comprehensive reviews on ore geology of this area (Dill, 1989, Dill et al. 2008a-see further literature cited there) (Fig. 1a–c). The present study is based on a combination of mineralogical and chemical data obtained during this investigation and collected from the literature, mainly KTB reports. KTB is the German abbreviation of "The Continental Deep Drilling Program of the Federal Republic of Germany" (1987–1995 which at the very end reached a final depth at 9101 m). The data relevant for economic geology, derived from all kinds of pre-well site and on-site examinations, have not been evaluated to the extent they deserve, because most emphasis was placed on geodynamic issues during the research program (Dill, 1989). This composite paper – review and study- aims at the following issues:

- Which are the controlling structural and lithofacial parameters of the carbonate-related metallic and non-metallic mineralizations?
- What is the physico-chemical regime of the different mineral associations made up of carbonate and calcsilicate minerals like?
- When did the mineralization form and how did these different carbonate-hosted mineral occurrences embedded into the overall ore mineralization evolve?
- To what extent have crustal and subcrustal processes had an influence on these mineral deposits?

To correlate the different types of carbonate-hosted mineralization and as a link to non-carbonate hosted mineral deposits in the region, the rare earth element contents (REE) are used as a minero-stratigraphical tool. Furthermore, they are also of assistance to constrain the origin of these deposits.

2. Methodology

The methodology has been only briefly treated because it is the routine application involving petrographic and ore microscopy, SEM-EDX/WDX and XRD as well as the chemical analytical tool XRF, all of which are well known or mentioned in the cited literature of the senior author (Dill et al., 2013). > 100 samples have been taken at outcrop, from abandoned mining galleries, open pits and drill cores, each weighing approximately 2 kg. Only the analytical methods for determination of the stable isotopes are cited here for completeness. The isotopic composition of oxygen and carbon was determined using an automated carbonate analysis device (GasBanch II) coupled on-line with a Delta "Advantage" (Finnigan, Germany) isotope ratio mass spectrometer (IRMS). In this technique, the samples react with phosphoric acid in separate vials and the resulted CO_2 is transferred with a continuous He stream, via an open split interface to the mass spectrometer. In order to assure a quantitative decomposition of the calcite – dolomite mixture, the powdered bulk rock samples were reacted at 72 °C for at least 4 h before the CO_2 was transferred into the mass spectrometer for measurement. Internal precision assessed by the standard deviation of 10 separate measurements was always better than 0.06 and 0.08‰ for $\delta^{13}C$ and $\delta^{18}O$, respectively. The external precision, based on the repeated measurement of a sample in different trials, was in the same range. Accuracy was checked by repeated measurement of the NBS19 calcite standard. The average of 15 measurements was

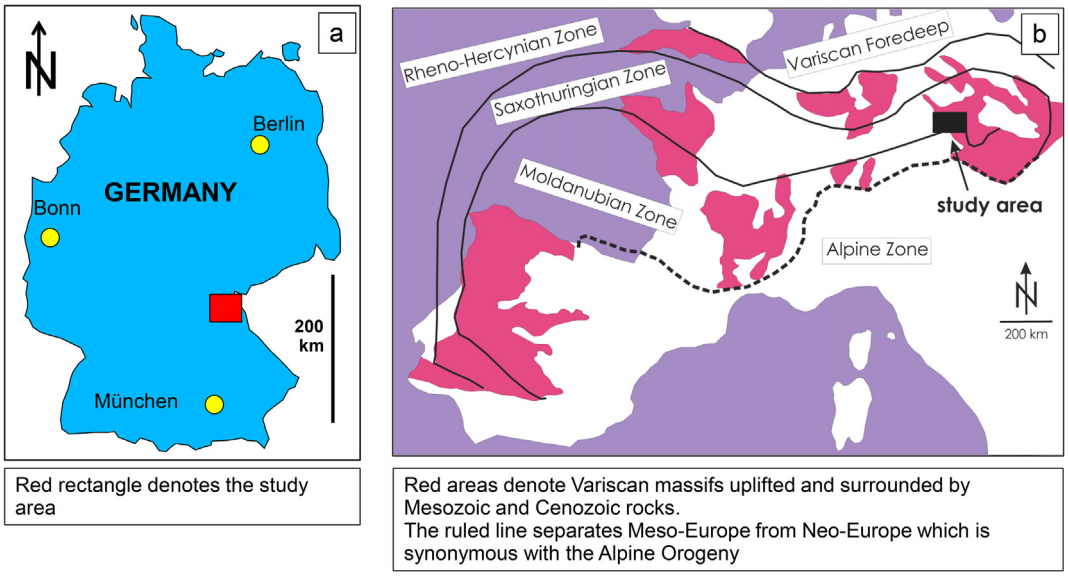

Fig. 1. The geological setting and the position of carbonate-hosted mineralization within and around the Fichtelgebirge Pluton, Germany. With an overview of the REE contents normalized to PAAS of some of the occurrences. The data is from this study unless stated otherwise. For more information, see also Table 1. The mineralized sites are given by white dots framed by full black lines. Green dots: mineralization with Sb minerals, framed by full brown line: mineralization with talc, framed by dashed line: mineralization with As minerals. FL = Franconian Line. a) The position of the study area in SE Germany. b) The position of the study area within the European Variscides. c) The position of the study sites around the Fichtelgebirge Pluton. (1) Brandholz-Goldkronach Sb-Au vein-type deposit with ankerite and dolomite. (2) Warmensteinach Ba-F vein-type deposit with siderite and dolomite. (3) Holenbrunn marble with calcite and minor dolomite, stratabound (brown). (4) Sinatengrün marble, with talc and Sb-As-Hg-Pb-Cu-Zn-Ni-Co-W-F mineralization. a) Graphite-bearing calcite marble (brown) plus calcite I (Hecht et al., 1999a) (red). b) Dolomite-bearing calcite marble (blue) plus dolomite I (Hecht et al., 1999a) (green). c) Dolomite-bearing calcite marble with talc, scheelite, strontianite (brown). d) Calcite-bearing dolomite calcsilicate-marble with talc (blue). e) Ankerite-bearing calcite calcsilicate-marble with talc and Cu-Pb-S mineralization (blue). f) Graphite-bearing calcite marble (brown) with Cu-Pb-Fe-Zn sulfide and fluorite mineralization. g) Mn-siderite bearing calcite marble (blue) with magnetite and ilmenite. h) Calcite marble (brown) with Sb-Hg-As-Cu sulfide and minor talc. i) Calcite encrustation (brown) with Cu sulfide and Ca-Fe phosphate, vein-type j) Ankerite-bearing calcite mineralization with Ni-Co arsenide (blue), vein-type k) Dolomite-bearing calcite mineralization with Cu-Fe-Pb arsenide and sulfide (red). (5) Göpfersgrün massive talc with W mineralization and Sb vein-type mineralization. a) Dolomite II marble (Hecht et al., 1999a) (brown), this study (red). b) Dolomite III marble (Hecht et al., 1999a). c) Calcite II marble (Hecht et al., 1999a) (brown)), this study (red). d) Calcite III marble (Hecht et al., 1999a). e) Calcite in talc ore with stibnite, apatite, gibbsite (red). (6) Thiersheim stratiform siderite deposit intercalated into calcitic dolomite marble with Cu-Fe vein-type mineralization. (7) Thiersheim massive halloysite deposit enriched in REE (brown). (8) Stemmas calcite marble (Hecht et al., 1999a) (red). (9) Arzberg, stratiform and stratabound siderite deposit with As-Cu-Zn-Pb vein-type mineralization. (10) Aign, stratiform siderite deposit with Cu mineralization. (11) Neusorg, stratiform siderite mineralization intercalated into calcitic marble (blue) with Cu vein-type mineralization. (12) Pullenreuth-Dechantsees, stratiform siderite mineralization intercalated into calcitic marble with Cu-F vein-type mineralization. (13) Tröstau stratiform siderite mineralization intercalated into calcitic marble with Zn vein-type mineralization. (14) Wurlitz, Sb-bearing calcite veins in metaultrabasite. (15) Hebanz, stockwork-like U-bearing calcitic episyenite. (16) Grossschloppen, stockwork-like to vein-type U-bearing quartz vein and episyenite. (17) Lengenfeld, stockwork-like U-bearing calcitic episyenite. d) Legend of the geological map of Fig. 1b. (For interpretation of the references to color in this figure legend, the reader is referred to the web version of this article.)

within ± 0.06 and ± 0.10‰ (1 s) of the certified δ values for carbon (1.95‰ PDB) and oxygen (−2.20‰ PDB), respectively.

3. Geological setting

The lithological units in the study area are part of the Saxothuringian Zone and the northern part of the Moldanubian Zone extending along the western edge of the Bohemian Massif, which is the core complex of the Central European Variscides (Franke, 1995; Franke et al., 1995). The oldest lithologies and structures are representative of a rift basin that evolved from the Cambrian, in parts as early as late Proterozoic, through the Ordovician (Linnemann, 2003; Kroner and Hahn, 2004). Initial spreading provoked arenaceous and argillaceous sediments of the neritic Thuringian Facies. These Paleozoic and Late Proterozoic sedimentary rocks host two horizons of calcareous rocks ("Wunsiedel Marble") (Fig. 1b and c). When the Saxothuringian ocean was subducted to the S beneath the allochthonous Teplá-Barrandian Zone during Early through Mid Devonian times, nappes stacked, leaving behind two klippen after erosion, one exposed at the SE edge of the study area in the Moldanubian Zone and the other in the Münchberg Gneiss Complex (Winchester and PACE TMR NETWORK TEAM, 2002) (Fig. 1b and c). In the aftermaths of the nappe emplacement and during the final collision, anatexis brought about a spade of Late Carboniferous to Permian granitic intrusions which the Fichtelgebirge is famous for and also is the centerpiece of the present study (Fig. 1b). According to Finger et al. (1997), the majority of these Variscan plutons is attributed to S-type granites made up of high-K and to I-type granitoids. During their comprehensive field and laboratory studies, Richter and Stettner (1979) singled out two different groups of granitoids, each of which with a specific trend of magma differentiation. The Older Granites cover the entire range from granodiorites through aplite granites with the majority of them plotting in the field of monzogranites, whereas the younger granite suite is made up of monzogranites grading into syenogranites which make up the lion share of this magmatic suite. The Older Granites spread the age interval 315.8 ± 0.2 to 321 ± 14 Ma and the ages of the Younger Granites range from 290 ± 4 to 301 ± 8 Ma – see compilation in Dill (2015a,b).

The felsic igneous intrusions are interpreted as a consequence of post-collisional extension and magmatic underplating in a zone of high heat flow. In the Fichtelgebirge Pluton, younger granites intruded into the older ones to the W of Wunsiedel, where they form a granite complex extending in NW-SE direction similar to the younger Erzgebirge granites at the eastern edge of the Fichtelgebirge-Erzgebirge Anticline (Budzinski and Tischendorf, 1985). Subsequently dolerite dykes were emplaced along NW-SE-striking fault zones while rhyolite dyke swarms occur towards the E along a deep-seated lineament, which

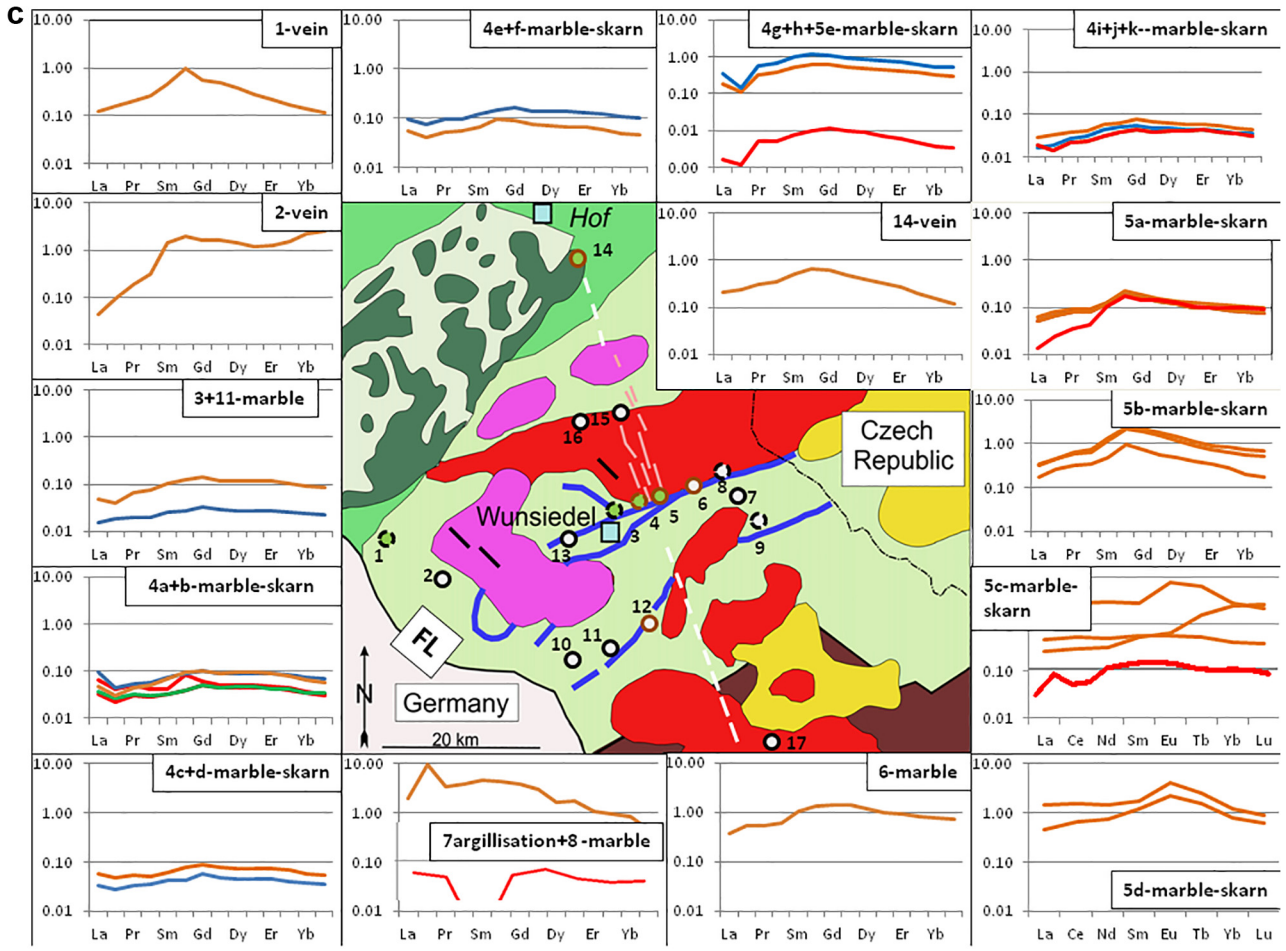

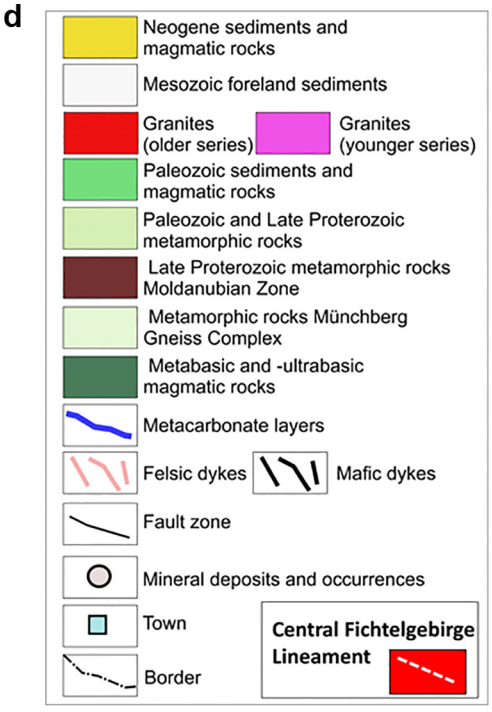

Fig. 1. (*continued*)

runs NNW-SSE (Fig. 1c). After a long period of time during which the study area fell dry and was encroached only upon by the Mesozoic Sea at its western margin, the basement was uplifted along a NW-SE trending deep-seated fault zone called Franconian Line (Fig. 1). Widespread deposition of terrigenous sediments took place during the Neogene when the Eger/Ohre Graben subsided. It was accompanied sporadically by the ascent of basic lavas and the expulsion of air fall tuffs.

4. Results and interpretation

4.1. Vein-type sulfide deposits with carbonate gangue in the wall rocks of granites

Three vein-type deposits with carbonate minerals as gangue reside in the wall rocks of the Fichtelgebirge granite pluton (Table 1, Fig. 1c – 1, 2, and 14).

The Sb-Au veins in the Brandholz-Goldkronach Mining District prevalently are oriented N-S, NNE-SSW, NE-SW and rarely NW-SE (Buschendorf, 1930; Jung and Hoell, 1982; Dill, 1985a,b). Their dip varies from 90° to 60°. Apart from carbonate minerals, the veins contain quartz associated with minor kaolinite, muscovite and chlorite. The carbonate minerals precipitated only in those veins with stibnite and quartz (Fig. 2a). Scheelite was found concentrated in vugs of the metabasic wall rocks of the Sb-Au veins.

The neighboring carbonate-bearing Ba-F veins at Warmensteinach are markedly different from the afore-mentioned Sb-Au veins in terms of structural geology as well as ore minerals (Fig. 1). They are oriented NW-SE and only have little Cu-sulfides (Table 1). The veins are abundant in ankerite and siderite and were of economic importance with regard to their fluorite and barite contents (Fig. 2b).

Scouting the Wurlitz ultrabasic rocks situated at the easternmost edge of the Münchberg Gneiss Complex for carbonate-hosted mineral assemblages in the course of this investigation identified small veinlets with calcite accompanied by stibnite (Fig. 2c). Pentlandite and pyrrhotite belong to the primary sulfide mineralization of the serpentinite-peridotite complex. Chalcopyrite is present in this primary mineralization and also in the younger veinlets (Table 1). Antimony in ultrabasic igneous rocks is a novelty for the region (Aral, 1989; Firstova et al., 2016). The Sb-sulfosalts at, e.g., Holenbrunn and Sinatengrün are dealt with later because they do not form vein-type deposits of their own but are only confined to the carbonate beds of the Wunsiedel Marble.

4.2. Stratabound carbonate-hosted deposits in the proximity of granites

4.2.1. The calcitic-dolomitic Wunsiedel marble

Along the southern edge of the Fichtelgebirge Pluton, several marble horizons line up collectively named as Wunsiedel Marble after the town of Wunsiedel at the heart of the Fichtelgebirge Mountains (Figs. 1 and 3a). Their age is still under dispute on account of lacking radiometric data and therefore, based on lithological and stratigraphic reasons, the age is constrained to the interval Late Proterozoic to Cambrian (Wurm, 1961). The major components of this well-bedded to massive marble are calcite and dolomite, which may diminish at the expense of calcsilicate minerals, e.g., tremolite. The sedimentary nature of these horizons is underscored by beds of phyllite and graphite schist alternating with the marble (Fig. 3a and b). The thickness of the marble beds varies from 150 to 200 m. A chemical study treating the Sr isotopes of marble and calcsilicate rocks of the Saxothuringian-Moldanubian transition zone also included the Wunsiedel Marble and came to following results (Wiegand et al., 1994). The major thermal event reflecting an isotopic homogenization during the Variscan orogeny is the LP/HT regional metamorphism at 319 + 36/−29 Ma in the temperature range between 680 °C and 600 °C (Wemmer and Ahrendt, 1993). The age supports the K/Ar cooling age of 312.5 ± 2.5 Ma when muscovite passed the 350 °C temperature isograde (Kreuzer et al., 1989). It also corresponds to the Rb/Sr whole rock age of the older granites 319 ± 3 Ma, which intruded immediately north of the Wunsiedel Marble and whose magma had a minimum temperature of 660 °C (Richter and Stettner, 1979).

4.2.2. Siderite beds

The Fe-bearing carbonate minerals, mainly siderite, are present in both metasedimentary rocks, in the marble and the calcsilicate rocks (Table 1 – see 3–6, 8–13). In some places, siderite beds are also found as offshoots penetrating into the metapelitic country rock, e.g., at Aign (Fig. 1c) or they form discrete ore bodies in the hanging wall or footwall rocks of the marble beds like in the Arzberg Fe ore deposit (Fig. 3b) (Von Horstig and Teuscher, 1979). In the afore-mentioned Fe deposit, both authors describe the marble horizons as well-bedded, whereas in the siderite ore body bedding has been reported as only vaguely expressed or totally absent. Carbonate forming concentric globular structures around nuclei of phyllite is held to be indicative of a metasomatic origin of the Fe concentration (Fig. 2d). At Tröstau, Fe deposit where calcsilicate rocks alternate with phyllite, different types of siderite ore can be established. The oldest generation (gen. 1) of siderite identified is characterized by equigranular aggregates of siderite, whose individual grains show undulous extinction due to subsequent deformation. Siderite of generation 2 infiltrated quartz clasts of the metapelitic country rocks along grain boundaries (Fig. 2e). A late-stage siderite (gen. 3), which can be distinguished from the overall collomorphous morphology fills vugs (Fig. 2f). The drusy texture attests to a deficit in fluid supply relative to the space provided for crystallization. Tröstau is one of the stratabound carbonate deposits which also contains rhodochrosite (Table 1). At Sinatengrün and Göpfersgrün, the Mn content of the mineralizing fluids was too small to create rhodochrosite and Mn-bearing siderite developed instead. Sinatengrün stands out from these carbonate deposits by the presence of strontianite (Table 1).

4.2.3. Sulfide-arsenide mineralization accompanying carbonate minerals

Excluding chalcopyrite, sphalerite, galena, arsenopyrite and pyrite, which may be traced along shear planes and found disseminated in the calcitic marble, the majority of sulfides and arsenides listed in Table 1 are spotted in the marble only on a microscopic scale (Fig. 4a). The minerals prevalently infill tension gashes or druses and vugs. The first detailed mineralogical investigation about the sulfide-arsenide mineralization was by Felser et al. (1965), which is supplemented in the current study.

The presence of Sb- and As-minerals reveals an antithetic trend along a W-E transect parallel to the Wunsiedel Marble from Holenbrunn to Thiersheim but perpendicular to the NNW-SSE striking Franconian Line (Figs. 1c, 3). It allows for a subdivision of the Sb-As mineralization in the metacarbonates into two facies groups as a function of their distance away from the Franconian Line that is highlighted by the felsic dikes (Fig. 3a). Where the structurally-controlled felsic dikes intersect the metacarbonates a barren zone devoid of Sb- and As-minerals can be recognized (Fig. 3a). The occurrences at Holenbrunn, Stemmas and Arzberg representative of the marginal facies have minerals lower in S contents (arsenopyrite: 46 wt% As, 16.7 wt% S) (Fig. 3a – grey squares 3, 8, 9). The central facies represented by Sinatengrün, Göpfersgrün and Thiersheim are lower in As but abundant in S (Cu-Hg-Ag-Sb fahlore: 4.6 wt% As, 16.6 wt% S) (Fig. 3b – blue squares 4, 5, 6). A similar order of abundance can be established for the Sb and S trends. In the marginal facies, the following Sb minerals occur (dyscrasite: 27.3 wt% Sb, 0 wt% S, gudmundite: 58.1 wt% Sb, 15.3 wt% S, jamesonite: 35.4 wt% Sb, 21.7 wt% S, meneghinite: 19.5 wt% Sb, 17.6 wt% S), whereas in the central facies the S content increases (Sinatengrün: dyscrasite: 27.3 wt% Sb, 0 wt% S, gudmundite: 58.1 wt% Sb, 15.3 wt% S, jamesonite: 35.4 wt % Sb, 21.7 wt% S, Göpfersgrün + Sinatengrün stibnite: 71.7 wt% Sb, 28.3 wt% S) (Fig. 4b). From the marginal to the central facies, the As contents decrease, in favor of the S contents. The Brandholz-Goldkronach vein-type deposit (Section 4.1) has to be placed in the marginal

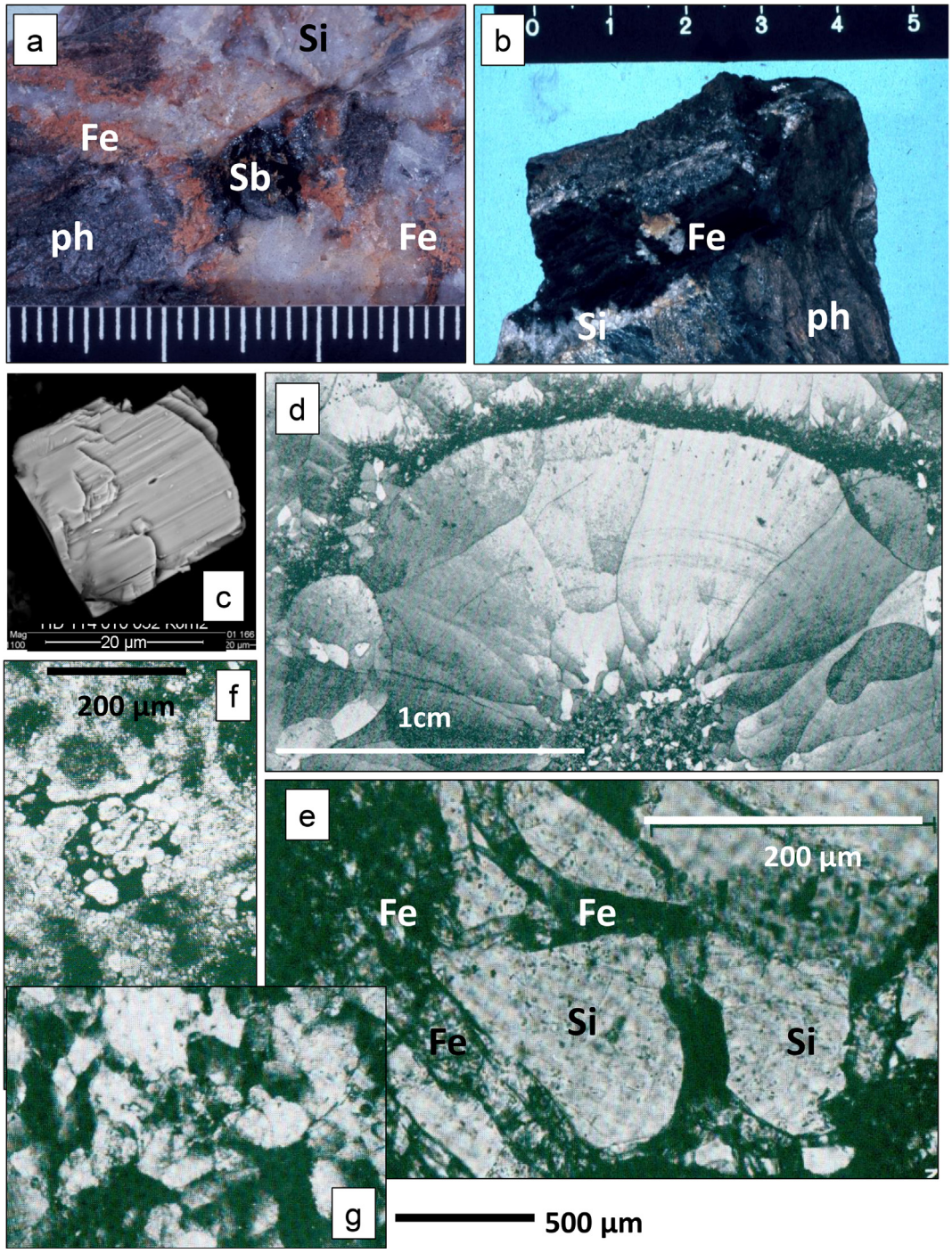

Fig. 2. Carbonate and ore minerals in different types of mineral deposits around the Fichtelgebirge Pluton. a) Carbonate gangue minerals at the selvage of one of the Sb-Au veins at Brandholz-Goldkronach. Si: quartz, Fe: siderite plus ankerite, Sb: stibnite, ph: phyllite. Width of image 3 cm. b) Black siderite (Fe) forms the youngest mineral in the quartz veins of the Warmensteinach Ba-F mining district intersecting Paleozoic phyllite (ph). c) Sheared stibnite crystal from the veinlets intersecting the metaultrabasic rocks at Wurlitz. d) Siderite metasomatically replacing limestone, starting from a nucleus of phyllite fragment. Arzberg Fe deposit. Thin section, cross polarized light (Von Horstig and Teuscher, 1979). e) Quartz (Si) clasts in metapelite country rocks adjacent to the calcsilicate rocks are infiltrated by siderite (Fe) along grain boundaries in the Tröstau Fe deposit. Thin section, plain polarized light. f) Vugs filled with collomorphous siderite of a low-temperature mobilization. Tröstau Fe deposit. Thin section, plain polarized light. g) Equigranular siderite aggregates showing undulous extinction as a result of deformation. Tröstau Fe deposit. Thin section, crossed polarized light.

facies with regard to the As- and S-contents of its mineral assemblage. As to the silver content an inner marginal facies can be distinguished from an outer central facies with Ag-sulfides like acanthite and Ag-Sb-As sulfides of the polybasite-proustite solid solution series (s.s.s.). Nickel-cobalt arsenides of the skutterudite s.s.s. diminish towards the margin. The subdivision of minerals into members belonging to the marginal and central facies, respectively, is based upon their proximity to the deep-seated lineamentary fault zone, characterizing the central facies, which strikes NNW-SEE and which is marked in the field by rhyolite and dolerite dykes.

Siderite was found in the wall rocks of the marble near Neusorg at a depth of between 90 and 100 m in a drill hole (Friedrich et al., 1988;

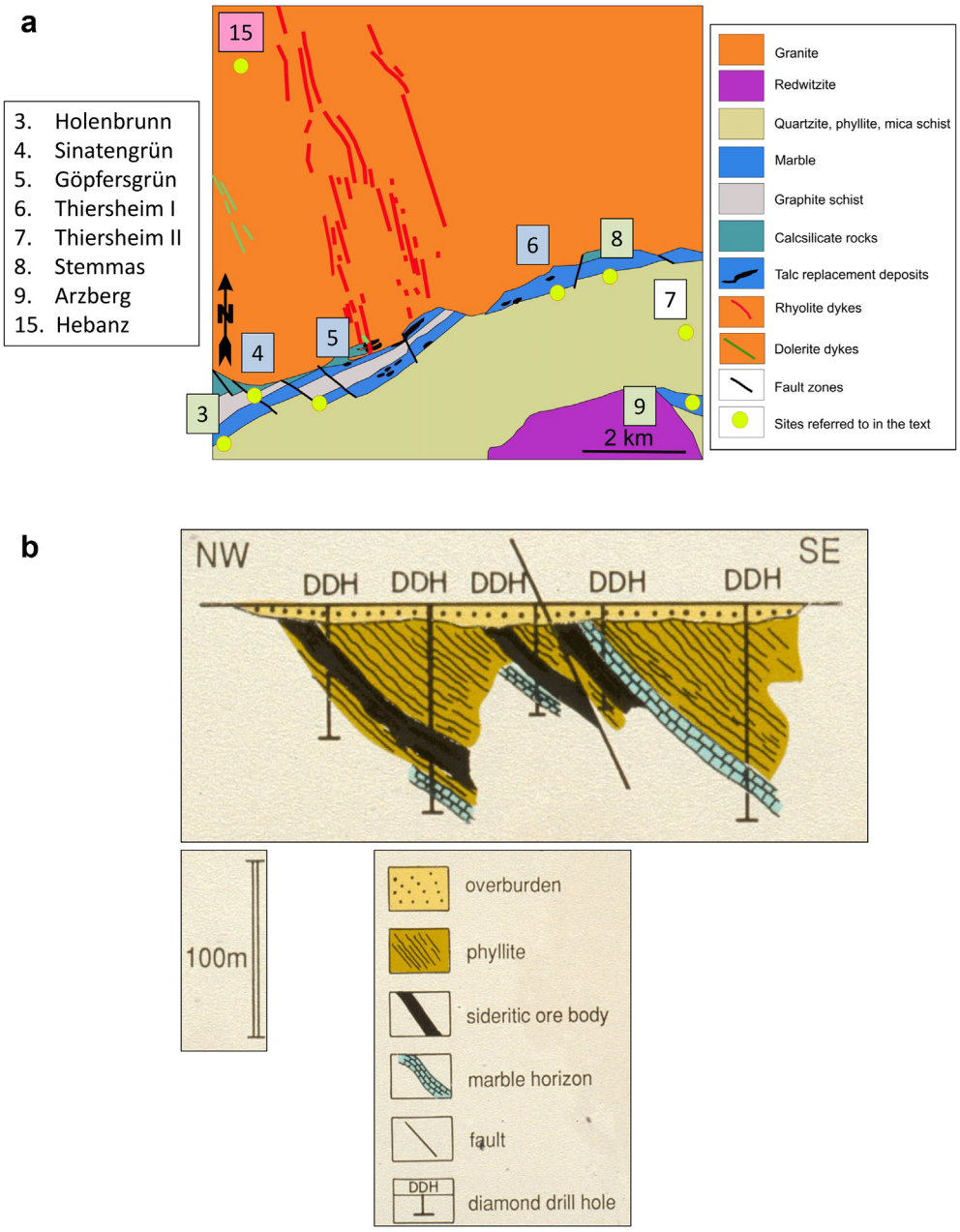

Fig. 3. Mineral associations bound to marble horizons adjacent to the granites and carbonate-related episyenitization within the granites. The numbers in the figures refer to the localities in Fig. 1. a) Geological setting of the Holenbrunn-Arzberg stratabound mineralization adjacent to the granite pluton and the intragranitic Hebanz episyenite. Geology modified from Wurm (1932) and Stettner (1959). b) Stratabound siderite ore deposit at Arzberg in cross section (Dill 1985a). c) The episyenite in a close-up view in relation to the fault system (above). The cartoon illustrates the position of the episyenite within the sequence of alteration from the unaltered granite to the uraniferous zone of silicification at Grossschloppen. For geological setting of Hebanz and Grossschloppen deposits geological map below.

Richter et al., 1988). Elevated As, Cu and Zn have been reported by Richter et al. (1988), i.e. from Neusorg which shows more affinity to the marginal facies. These anomalously high values are not exclusive to the metacarbonates but also encountered in the metapelites. In addition to the common Cu-Pb-Zn minerals, glaucodot and bravoite were reported as Ni-Co-As-S minerals (Friedrich et al., 1988). Molybdenite does not reflect any facies-bound emplacement. Bismuthinite, however, tends to be concentrated in the central facies. Chalcopyrite and its supergene alteration products, e.g., covellite and chalcocite are the most common Cu sulfides in the study area, only at Holenbrunn and Sinatengrün minor amounts of cubanite are associated with chalcopyrite.

4.2.4. W-Ba-F Mineralization accompanying carbonate minerals

Scheelite is a member of the skarn mineralization of the central facies at Sinatengrün and Göpfersgrün where it is found as porphyroblasts in a vesuvianite skarn barren as to the powellite component (Fig. 4c). Barite and fluorite do not show any facies-bound distribution in the calcareous stratabound deposits (Fig. 4d). Purple fluorite in nests of the marble is intergrown with chalcopyrite and plates of hematite ("specularite").

4.2.5. Silicates accompanying carbonate minerals

The silicate minerals diagnostic for the alteration of the Wunsiedel Marble are subdivided into two groups, the Ca-Mg-Fe-Be silicates which characterize an early stage of alteration while the phyllosilicates are typical of the late-stage alteration (Table 1).

Ca-Mg-Fe-Be silicates: Tremolite is the most common Ca-Mg-Fe silicate in the marginal and central facies (Fig. 4e). Less widespread than

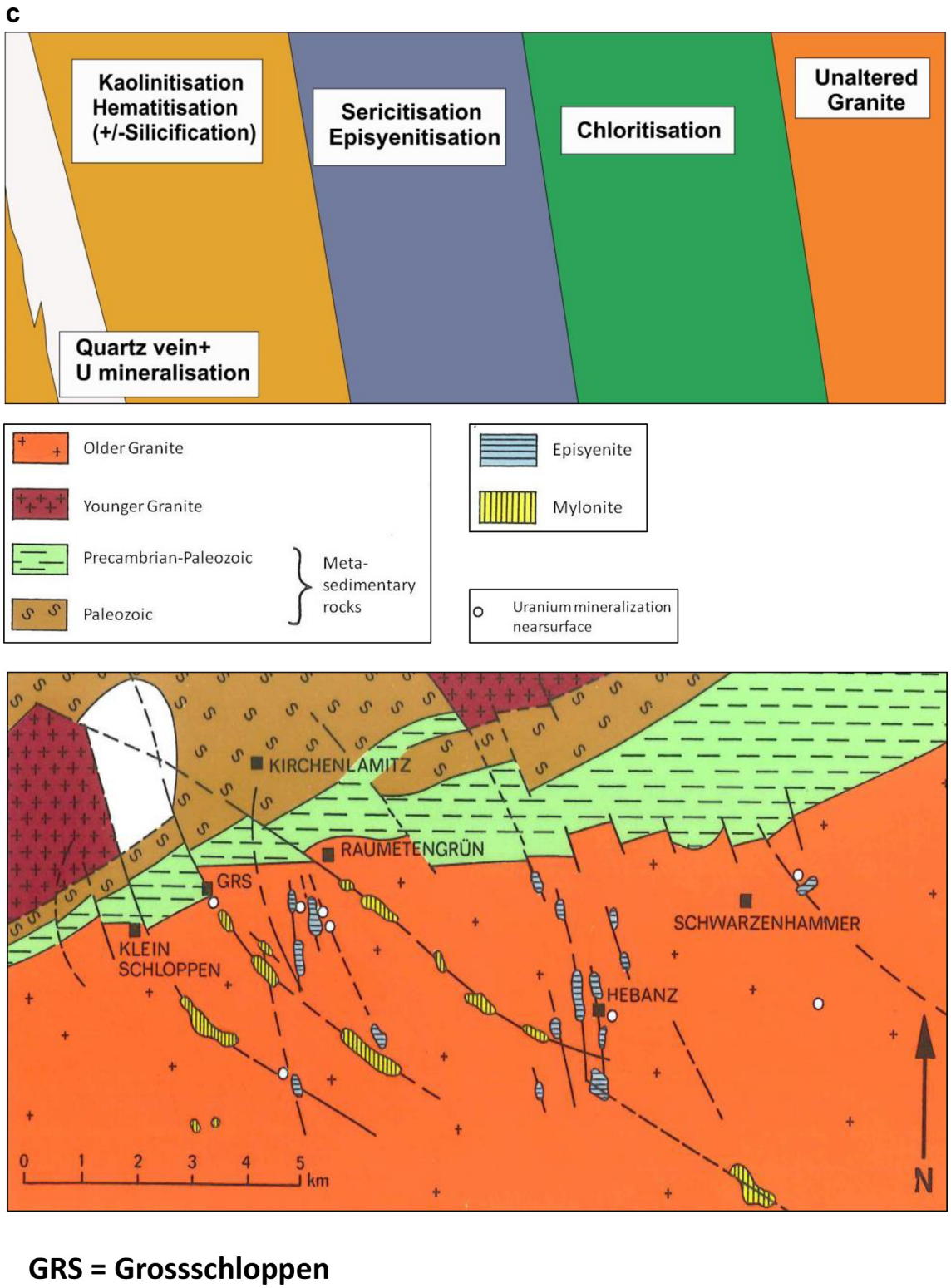

Fig. 3. (*continued*)

the well-shaped tremolite, grossular, titanite and vesuvianite developed in both facies types along the southern edge of the pluton. Silicates of the clinozoisite-epidote s.s.s. and diopside are confined to the central facies and the western part of the marginal facies proximal to the central facies, e.g., Holenbrunn. This site also contains some prehnite. Beryl is a rare mineral and exclusive to the marble in the talc deposit at Göpfersgrün, where it is found at the zone of intersection of the marble by aplite dikes.

Phyllosilicates: Among the sheet silicates of the argillic alteration zone of the marble, talc stands out because of its concentration at an economic level. An in-depth investigation of its geology was done by Stettner (1959) and a special study devoted to the dolomite and calcite minerals using REE, C-, O- and Sr- isotopes was performed by Hecht et al. (1999a). Talc has the chemical composition ($Al_{0.06}$, $Fe_{0.08}$, $Mg_{2.86}$) ($Si_{3.91}$ $Al_{0.09}$ O_{10}) $(OH)_2$ and is intimately intergrown with Mg-enriched chlorite. It forms a massive pale green rock which is easily distinguished

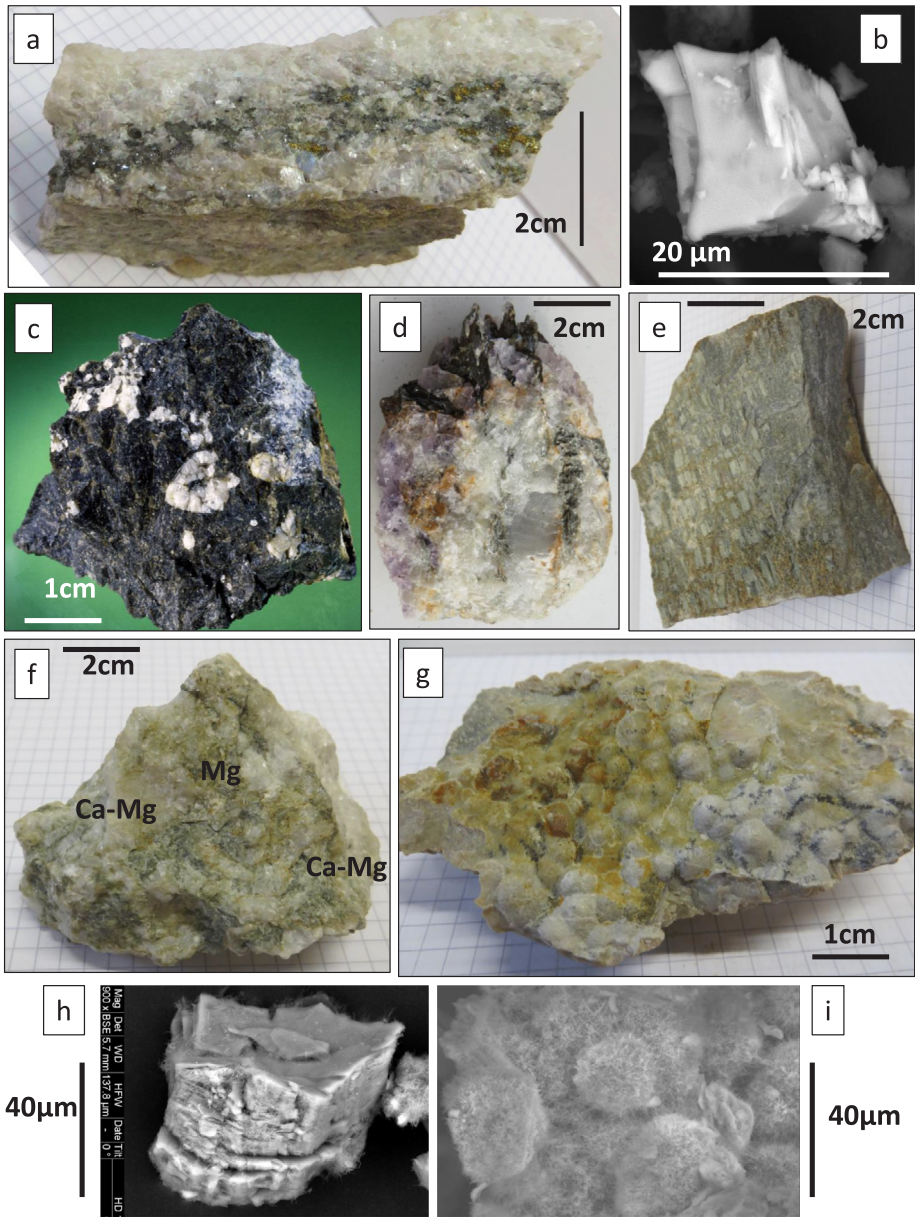

Fig. 4. Texture and morphology of non-carbonate minerals associated with Fe-Mg-Ca-Mn carbonate in stratabound deposits. a) Chalcopyrite, sphalerite, galena and covellite disseminated in calcitic marble at Sinatengrün. b) Flattened stibnite aggregates in the marble at Göpfersgrün. c) Porphyroblasts of Mo-free scheelite in vesuvianite skarn at Göpfersgrün. d) Purple fluorite intergrown with hematite ("specularite") and chalcopyrite in the marble deposit at Pullenreuth-Dechantsees-Kalkhaus. e) Talc-bearing marble with oriented plates of tremolite, Thiersheim 1. f) Massive greenish white talc ore (Mg) which as replacement of calcitic and dolomitic marble (Ca-Mg), Sinatengrün. g) Collomorphous talc of the late-stage metasomatism at Göpfersgrün "Johanneszeche". h) Concertina-texture of platy REE-enriched halloysite from Thiersheim 2. i) Globular aggregates made up of tubular halloysite, Thiersheim 2. See also globules of talc in (g). (For interpretation of the references to color in this figure legend, the reader is referred to the web version of this article.)

from the gray dolomite-calcite gangue (Fig. 4f). According to Stettner (1959), Al-enriched chlorite (leuchtenbergite - sheridanite) is replaced by Al-poor pennine. The latest stage of Mg-metasomatism resulted in the formation of globular collomorphous soapstone (Fig. 4g). Talc was concentrated only in the zone between Sinatengrün and Thiersheim and found sporadically at Pullenreuth-Dechantsees (Table 1, Figs. 1c, 3a). The latter subeconomic talc occurrence is located in the southward prolongation of the Franconian Line (Fig. 1c). Muscovite, phlogopite and vermiculite, which reflect a transitional alteration stage of biotite, are precursor phyllosilicates relative to the formation of soapstone, whereas kaolinite and smectite-group minerals developed subsequently. The rare regular mixed-layer phyllosilicate corrensite marks the alteration of chlorite-group minerals into smectite-group minerals. In this context an almost monomineralic halloysite deposit strongly enriched in LREE formed in amphibolite and gneiss, named Thiersheim II, but is not bound to metacarbonate host rocks (Fig. 1c, 4h, 4i). The extraordinary halloysite deposit was mined in the past and lies halfway between the northern and the southern branch of the Wunsiedel Marble. There is no argillaceous mineralization comparable to it elsewhere in the NE Bavarian Basement. The surface expression of the deposit has an ENE-WSW orientation cut by a NW-SE trending fault zone. Halloysite has a similar chemical composition as kaolinite but contains additional water molecules between the layers, leading to the formula $Al_2Si_2O_5(OH)_4{\cdot}2H_2O$ in its fully hydrated form (Dixon and McKee 1974; Weaver, 1989; Joussein et al., 2005; Churchman et al., 2010). This phyllosilicate shows a tubular hydrated morphology as well as spheroidal plates which both can be recognized in the deposit (Fig. 4h, I – see also next line). There exists a striking resemblance between the globular talc and the hydrated form of halloysite (Fig. 4g and i).

4.3. Stockwork-like carbonate mineralization ("episyenite") within granites

"Skeletal granite" is a common term applied to rocks, which suffered from pervasive desilicification and eventually resulted in porous and vuggy rocks with a syenitic composition. They are barren of quartz and enriched almost only in alkaline feldspar (chessboard albite). The technical term "skeletal granite" can be adjusted to the international terminology and named accordingly as episyenite (Leroy, 1978). The increase in porosity and permeability renders episyenite suitable as

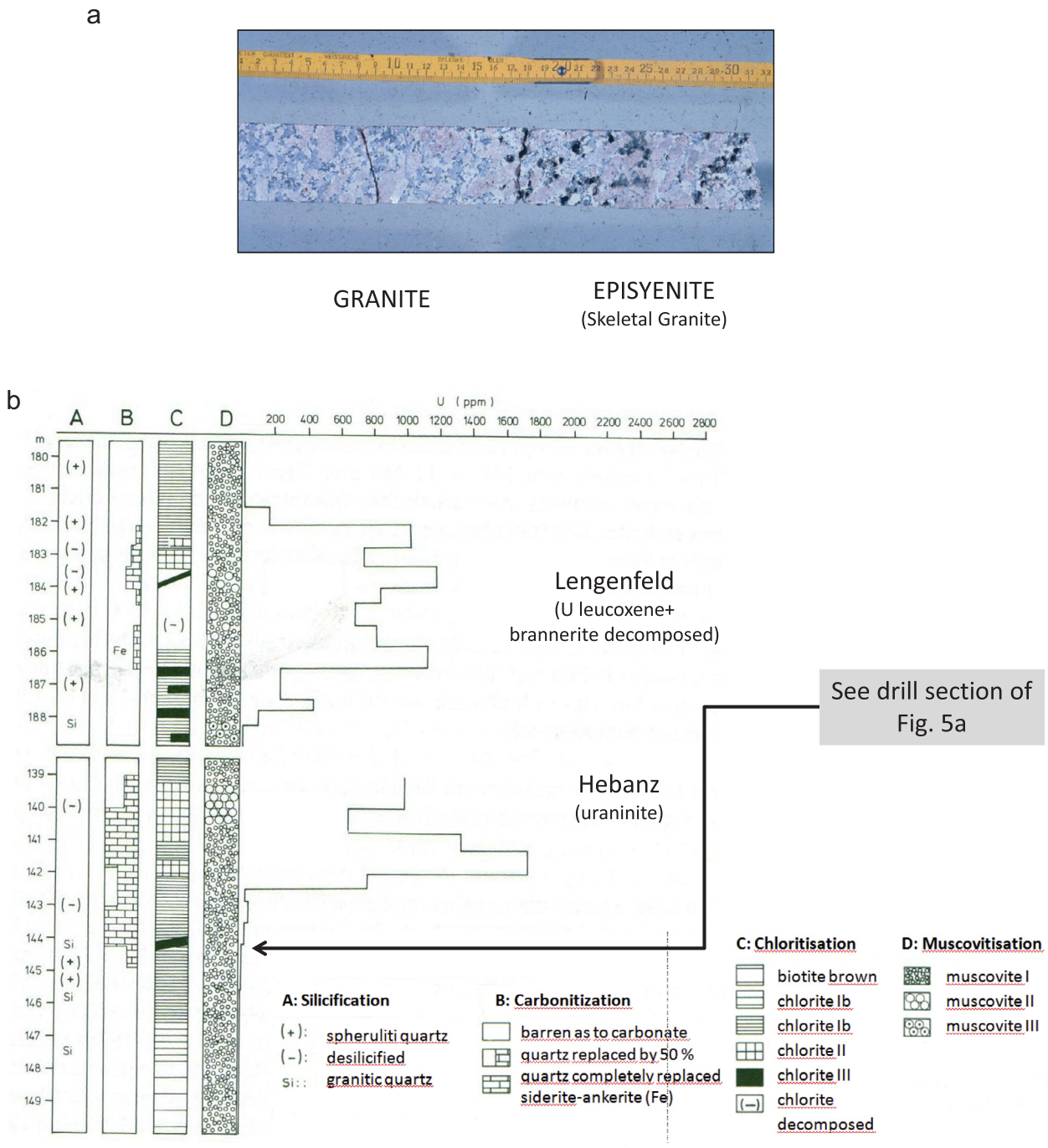

Fig. 5. Carbonate-bearing episyenites hosted by the older granites. a) Core section of the transition zone from a hematized porphyritic granite into a porous calcitic episyenite at the Hebanz U deposit (for position in the DDH 11 see b arrowhead). For location in the pluton, see Figs. 1c and 3c. b) The lithology and mineralogical composition of the Lengenfeld and Hebanz U-bearing episyenites (for location see Fig. 1c).

reservoir rocks for a wide range of elements and minerals such U, REE, Au and talc some of which may achieve economic grade as demonstrated in the Bohemian Massif by the Okrouhla Radouň episyenite-hosted U deposit, Czech Republic (Petersson and Eliasson, 1997; Recio et al., 1997; Hecht et al., 1999b; Borges et al., 2009; Dosbaba and Novák, 2012; Dolníček et al., 2013; López-Moro et al., 2013) (Fig. 5a). Apart from calcareous replacement minerals such as calcite, dolomite and siderite, different silicates can be observed Potassic metasomatism lead to white mica in the desilicified rock in the sericitised granites of the Água Boa Pluton in the Pitinga tin province, Amazonian Craton, Brazil (Borges et al., 2009). By contrast to this, Dosbaba and Novák (2012) reported quartz replacement by talc in the Věžná I pegmatite, Czech Republic, hosted by serpentinized harzburgite. The latter variety furnishes clear evidence that carbonate episyenitization in the in the granite is genetically equivalent to the talc replacement deposits at its marginal zone (Section 4.2.5, Figs. 1c, 3). Three examples frame the geological setting of the episyenitization found within the Fichtelgebirge Pluton at Hebanz as well as at Grossschloppen and within the Falkenberg Granite at Lengenfeld, which formed contemporaneously with the afore-mentioned older granites of the Fichtelgebirge Pluton (Figs. 1, 3, 5b). The Hebanz episyenite falls in the sub-group calcite episyenite, the Lengenfeld episyenite is attributed to the siderite/

ankerite-calcite episyenite (Fig. 5b). Outside the study area in the Höhenstein U deposit, the episyenite is dolomitic, whereas those episyenites with their vugs and pores mineralized with heulandite and stilbite are barren as to U (Dill, 1983). The carbonate mineralization in the episyenites is accompanied by chloritisation, which mirrors the decomposition of biotite following a specific decomposition path: Ia: green biotite with traces of 14 Å and 7 Å chlorites, Ib: Fe-Mg chlorite, II: Fe chlorite with interplanar spacing of 14 Å and 7 Å chlorites, III: on hairline cracks unaccompanied by Ti oxides. By contrast to the Hebanz and Lengenfeld U deposits, which are pure episyenites hosting a monotonous U mineralization only, the dolomite-calcite episyenitization at the Grossschloppen U deposit forms an integral part of a complex alteration zone made up of 5 distinct alteration zones: I: Unaltered granite, II: chloritisation, III: sericitisation/muscovitisation – episyenitization, IV: kaolinitisation – hematitisation (plus minor silicification), V: silicification/ quartz vein plus U mineralization (Fig. 3c).

Episyenitization occurs in zone III followed towards the center of the shear zone by silicification, which becomes more intense away from zone II towards zone IV where it reaches its climax with the emplacement of a quartz vein (Fig. 3c). In the opposite direction towards the margin, the desilicification is associated with newly formed star-shaped quartz aggregates, also observed in the Göpfersgrün talc deposits and the Lengenfeld and Hebanz episyenites, which is another hint to the contemporaneous formation of talc replacement and calcitic episyenite. Grossschloppen is the largest U deposit with the most variable mineral association (uraninite, coffinite, pyrite, chalcopyrite, klockmannite, umangite, clausthalite, guanajuatite (?), fluorite, little barite, native copper, chalcocite, covellite and a varied group of supergene U minerals). Fig. 3c illustrates the variation of episyenitization and mylonitic shear zones as a function of strike. Episyenites developed along NNW-SSE trending fault zones, while mylonitic shear zones are oriented NW-SE. On a regional scale, episyenitization is controlled by the Franconian Line (Fig. 1c).

4.4. Whole-rock chemistry of carbonate mineralization

The whole-rock geochemistry of two groups of carbonate-bearing mineral assemblages in the study area is investigated and the geochemical data are normalized to reference rocks. The first group encompasses calcsilicate rocks and marble which are treated in relation to unmetamorphosed calcareous rocks to constrain the parent rock of these metacarbonate rocks (Wunsiedel Marble). Strictly speaking, this approach has been taken to determine the allochemical and isochemical processes conducive to these metacarbonate rocks (Fig. 6). The second group consisting of different mineral deposits from calcitic episyenites to talc replacement deposits in dolomitic marble is normalized to a calcitic vein mineralization encountered in ultrabasic igneous rocks at Wurlitz (Figs. 1c-14, 7).

4.4.1. Marble beds and calcsilicate skarn deposits

Samples from the marble and calcsilicate-skarn-type rocks are normalized to impure marine limestones derived from different sites in the Persian Gulf region, from Thailand and Germany taken by the senior author. Classification schemes of limestones, which pay attention to the mineralogical composition, are based on dolomite, calcite and non-carbonate minerals (Leighton and Pendexter, 1962) (Fig. 6). Spider diagrams reveal the depletion and enrichment of major and trace elements of a lithology relative to a standard in the most striking way (Figs. 6a–c, 7). The data are plotted on a logarithmic scale with the “red ring” denoting the reference line 1; data < 1 denote chemical depletion, whereas data > 1 show enrichment of elements relative to the reference. Normalized to impure limestones (Fig. 6a), the Wunsiedel Marble is significantly enriched in Ca, Mg and Mn, with the best match between the marble and the pure limestone (Fig. 6b) and the calcsilicate-skarn and the impure limestones (Fig. 6b). Phosphorous is in both cases significantly enriched.

4.4.2. Structurally controlled carbonate-bearing and -hosted mineral deposits

Calcitic episyenite, carbonate-hosted Fe deposits, vein-type carbonate-bearing mineral associations and carbonate-hosted talc deposits are normalized to calcitic veinlets in ultrabasic igneous rocks from Wurlitz (Figs. 1c, 7), because all of them have in common the structural control of their mineral assemblages. Correlating the major elements of the carbonate-bearing mineral deposits along this NNW-SSE striking lineamentary fault zone with the reference mineralization from the ultrabasic igneous rocks shows the best fit top-down in Fig. 7 from the episyenites to the vein-type deposits. The trace elements are the visual expression of the ore mineralization found in each of these mineral deposits. The episyenites are abundant in U and the stratabound Fe deposits have a minor base metal mineralization aside of the main Fe concentration. The talc- and vein-type deposits are non-metallic deposits with mainly, fluorite which is not displayed in the diagram. Slightly elevated Cu, As and Bi contents are only of mineralogical relevance.

4.5. Rare earth element variation

4.5.1. Vein-type sulfide deposits with carbonate gangue

The REE pattern of hydrothermal carbonate systems has among others been investigated and summarized by Debruyne et al. (2016), including further detailed references. A comparison with vein-type mineral assemblages in NE Bavaria, bearing carbonate gangue minerals is given in Fig. 8 showing the variation of REE while the REE contents are listed in Table 2 (Dill et al., 1986, 2011). The position of mineral assemblages taken for reference is illustrated in Fig. 9.

Brandholz-Goldkronach: One sample from Brandholz-Goldkronach was analyzed for its REE content. The PAAS-normalized pattern shows a roof-shaped pattern with a maximum at Eu. The light and heavy REE (LREE and HREE) in the carbonate vein are equally depleted with respect to PAAS. The overall enrichment of the middle REE (MREE) in the carbonate bulk samples is atypical for carbonates and can be explained by a contribution from barite or scheelite, which both are commonly enriched in MREE. However, Hecht et al. (1999a,b) show similar roof-shaped REE patterns for their separates of hydrothermal carbonates, which they interpret as signature from hydrothermal alteration.

Warmensteinach: The sample of the Warmensteinach vein is depleted in the LREE with respect to PAAS, with values increasing to Sm and a flat pattern for the MREE and HREE. The pattern is similar to the Brandholz-Goldkronach vein except for the HREE, which can be explained to have been added to the vein mineralization by fluorine-bearing fluids.

Wurlitz: The sample from Wurlitz is an altered ultramafic rock with a roof-shaped PAAS-normalized REE pattern. This pattern is similar to that of Brandholz-Goldkronach and interpreted to have resulted from hydrothermal alteration.

4.5.2. Stratabound carbonate-hosted deposits

A general overview of REE from hydrothermally influenced marine systems was published by Klinkhammer et al. (1983). The PAAS-normalized REE pattern of the Holenbrunn sample is relatively flat, with a slight depletion of the LREE. The eleven skarn and vein samples from Sinatengrün were analyzed in this study and are compared to three samples from the same site analyzed by Hecht et al. (1999a,b). Their PAAS-normalized REE patterns are all similar, relatively flat and slightly depleted in LREE. Three samples from Göpfersgrün have been analyzed in this study and are compared with ten data from Hecht et al. (1999a,b). The REE patterns of the different samples vary, with 5a and b having a roof shape, 5c being variable, 5d showing a LREE-enriched roof shape and 5e having a depleted flat pattern with negative Ce anomaly (Fig. 1c).

Thiersheim I: Only one sample from this locality was analyzed, and the PAAS-normalized REE pattern is flat with LREE depletion and a

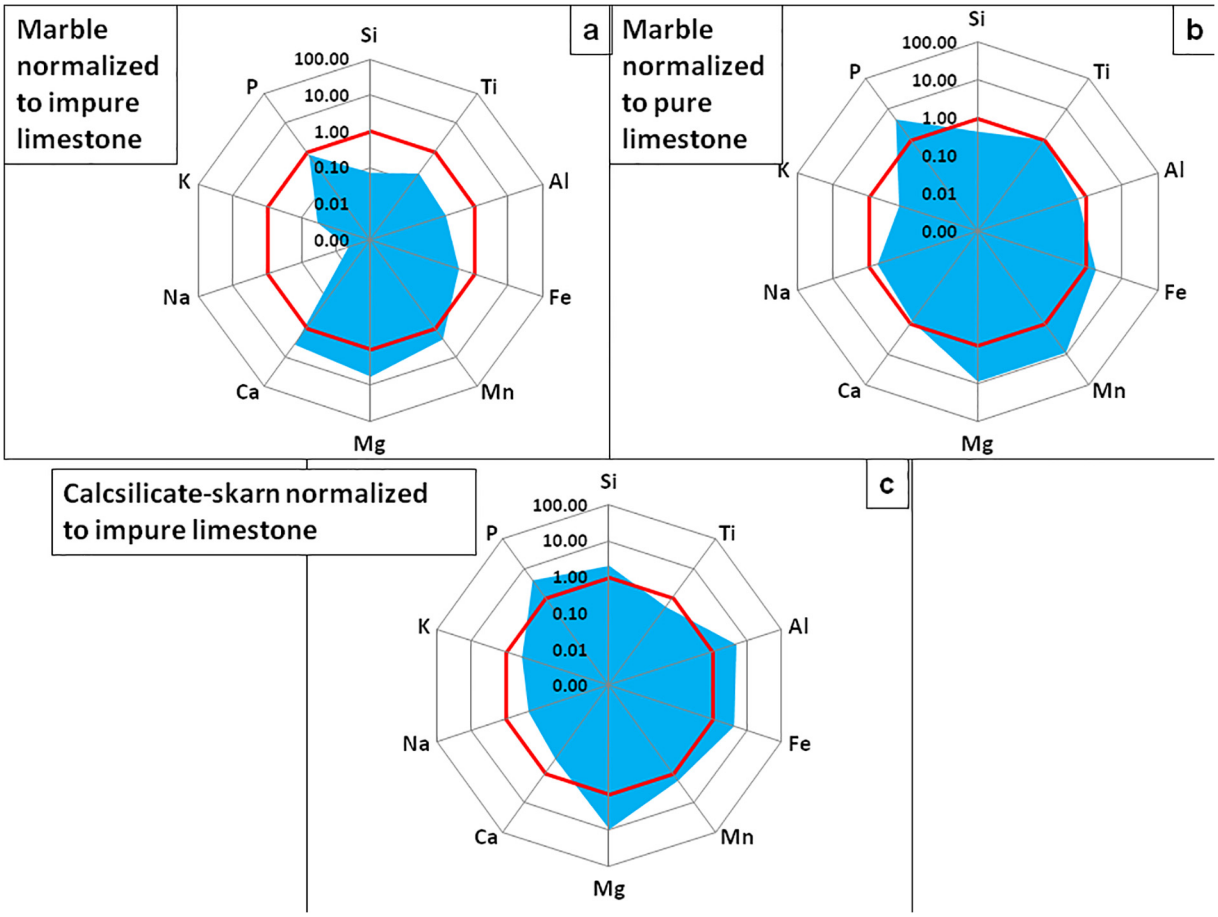

Fig. 6. Marble beds ("Wunsiedel Marble Beds") normalized to impure and pure unmetamorphosed limestones and calcsilicate-skarn (see also Figs. 1c, 3). a) Marble normalized to impure limestone. b) Marble normalized to pure limestone. c) Calcsilicate-skarn normalized to impure limestone.

slight enrichment of MREE.

Thiersheim II: This sample is characterized by the presence of halloysite. The REE pattern resembles typical patterns for halloysite, the main mineral of this sample (De Putter et al., 2002). It has a positive Ce anomaly, is relatively rich in the MREE and shows a steady fall from Eu to Lu.

Neusorg: The sample from Neusorg shows a flat PAAS-normalized REE pattern similar to the unaltered Wunsiedel Marble wall rock. The REE data lacks a negative Ce anomaly but shows a weak positive Eu anomaly.

4.6. Carbon and oxygen isotope variation

Brandholz-Goldkronach: Calcite and dolomite have been analyzed from this mineralized site. The $\delta^{13}C$ (VPDB) and $\delta^{18}O$ (SMOW) values of its carbonate minerals vary only slightly around −13‰ and 15.5–16.0‰, respectively (Fig. 10). These values overlap with those of calcite 3 from Hecht et al. (1999a,b).

Warmensteinach: The $\delta^{18}O$ values of calcite and dolomite from Warmensteinach are similar to those from Brandholz-Goldkronach, but $\delta^{13}C$ are higher at −8.76 to −8.99‰.

Holenbrunn: The two calcite separates from Holenbrunn vary strongly in their isotopic composition both, for oxygen and for carbon: (1) sample 11401219 has $\delta^{13}C$ of −2.15‰ and $\delta^{18}O$ of 11.82‰; and (2) sample 11401239 has $\delta^{13}C$ of −7.92‰ and $\delta^{18}O$ of 22.00‰.

Sinatengrün: Eleven samples from the Sinatengrün area have been analyzed. Their $\delta^{13}C$ and $\delta^{18}O$ composition varies similar to the calcite samples from Holenbrunn and cluster together with those in two fields in a $\delta^{13}C$-$\delta^{18}O$ diagram (Fig. 10). One group of samples yields $\delta^{13}C$ of 0.5 to −3.5‰ and $\delta^{18}O$ of 14.0–16.5‰, the second group yields $\delta^{13}C$ of −8.5 to −9.5‰ and $\delta^{18}O$ of 23–24‰. The second group of samples has similar $\delta^{13}C$ values as samples from Warmensteinach, but are heavier in their oxygen isotopic composition. Heavy oxygen isotope compositions of > 20‰ $\delta^{18}O$ have not been reported from the area (Hecht et al., 1999a,b).

Göpfersgrün: The calcite and dolomite separates from this area yield similar data, with $\delta^{13}C$ values of −2.79 and −2.58‰, and $\delta^{18}O$ values of 11.93 and 11.19‰, respectively. These values overlap with data for dolomite$_3$ from Hecht et al. (1999a,b).

Thiersheim I: The calcite and dolomite separates yield only slightly different data, with $\delta^{13}C$ values of –5.15 and –3.61‰, and $\delta^{18}O$ values of 11.76 and 12.03‰, respectively. They also overlap with data for dolomite$_3$ from Hecht et al. (1999a,b) and plot closely together with the first group of samples from Sinatengrün.

Neusorg: The calcite separate from Neusorg yields $\delta^{13}C$ values of 1.18‰ and $\delta^{18}O$ values of 21.50‰ well within the characteristic field for marble and limestone compositions.

Wurlitz: The calcite and dolomite separates yield only slightly different data, with $\delta^{13}C$ values of −2.47 and −2.77‰, and $\delta^{18}O$ values of 12.61 and 14.55‰, respectively. They overlap with data for dolomite$_3$ from Hecht et al. (1999a,b) and plot closely together with the first group of samples from Sinatengrün.

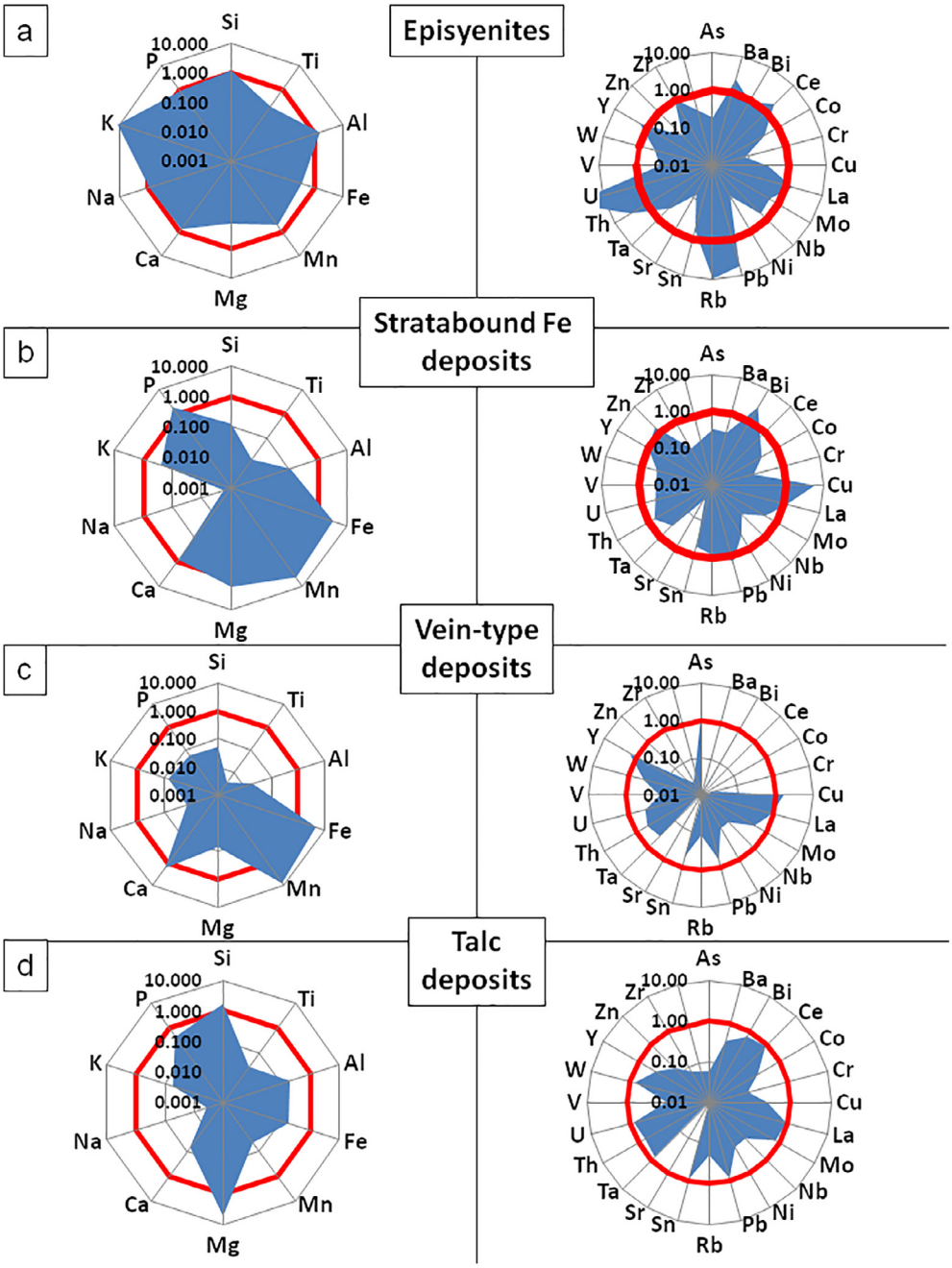

Fig. 7. Spider diagrams of mineralized sites normalized to calcitic veinlets in ultrabasic igneous rocks at Wurlitz (Fig. 1c, No 14). a) Calcitic episyenites. b) Stratabound carbonate-hosted Fe deposits. c) Vein-type carbonate-bearing mineral associations. d) Carbonate-hosted talc deposits.

5. Discussion

5.1. Rare earth elements (REE) the source of fluids and the way of concentration

Fluorite occurs in vein-type deposits together with Fe carbonate and in the marble beds accompanied by different carbonate minerals (Table 1). The fluorite mineralization in the immediate surroundings of the granites are discussed in relation to some other vein-type fluorite mineral associations along the western edge of the Bohemian Massif (Figs. 8 and 9). A comparison of the x-y plots by eye in Fig. 8 reveals that carbonates and halogenides in the vein-type deposits share the same parental fluids (see Warmensteinach). This is also corroborated by the La/Lu ratios and the calculated Eu anomaly. According to Bau (1991) and Bau and Möller (1992) strong complexation of HREE in alkaline fluids abundant in ligands is conducive to a La/Lu ratio smaller than 1, e.g., Warmensteinach and Neusorg. The reference types from the Lichtenberg-Issigau mining district, in which fluorite is associated with calcite, dolomite, siderite and ankerite, most closely resemble the Warmensteinach deposit (2). Where did the elements in the carbonate-bearing veins come from, from granitic rocks or metapelitic rocks? Möller and Giese (1997) and Irber et al. (1998) studied in detail the REE distribution between igneous and metamorphic rocks and their leachates contributing to the origin of fluorite mineralization. Fluorite associated with granite magmatism is characterized by a flat to LREE-depleted REE pattern that has a negative Eu anomaly (Gagnon et al., 2003). Negative Eu anomaly is found in most PAAS-normalized REE patterns from Nabburg-Wölsendorf (Ernst & August, Saltendorf), some of which have been taken as reference in this study. According to the studies of the afore-mentioned authors, fluids derived from granites are

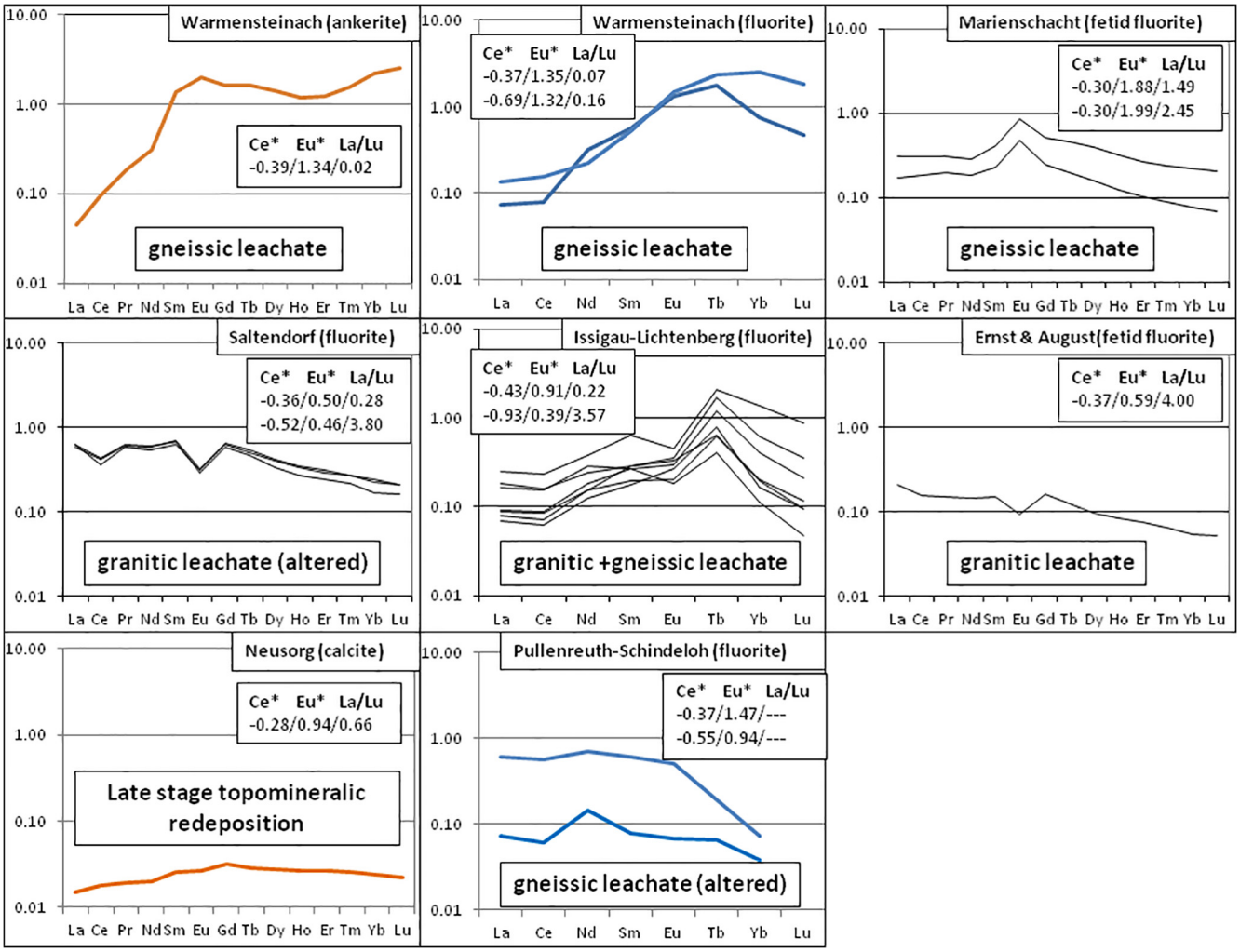

Fig. 8. REE data of fluorite and carbonate minerals normalized to PAAS. Diagrams given in bold-faced brown and blue lines from this study. Diagrams given in thin lines for reference are from Dill et al. (1986, 2011). Ce* = Cerium anomaly, Eu* = Europium anomaly, La/Lu = fractionation of LREE/HREE. (For interpretation of the references to color in this figure legend, the reader is referred to the web version of this article.)

characterized by more or less pronounced negative Eu anomaly, whereas leachates derived from gneiss create a positive Eu anomaly (Fig. 8). Fluids originating from a gneissic or metapelitic source display a lower La/Lu ratio in the majority of cases than fluids of granitic leachates. With this in mind and based on visual inspection as well as a comparison of the Eu anomaly, the Warmensteinach (2) carbonate-fluorite system was supplied with fluids interacting with gneissic rocks at depth. In the adjacent Lichtenberg-Issigau carbonate-fluorite mineral association, a dual source can be envisaged. The apical parts of granite have been proven by drilling at a depth of between 261 and 516 m below surface.

The age of formation of the vein-type fluorite mineralization can only be performed based on mineralogical and geological circumstantial evidence. Dolníček and Slobodník (2001) and Wolff et al. (2016) provided the most recent age information from fluorite deposits situated across the Czech-German border. Two fluorite samples from the Horni Krupka, Czech Republic, with ca. 170 °C and ca. 43 °C closure temperatures yield different (U–Th–Sm)/He ages of 290 ± 10 Ma and 79 ± 10 Ma, respectively (Wolff et al., 2016). The authors interpret the data such as the mineralizing fluid system was active from the Early Permian through the Late Cretaceous. The most recent members of this mineralizing system are unrelated to a granitic heat source, but driven by a subcrustal thermal event, which is controlled by the deep-seated structures illustrated in Fig. 9. The NW-SE striking fractures observed in the granite core of Weißenstadt geothermal well (1835 m) form the conduits for a fluorine-enriched Na-Ca-Cl-SO_4 fluid system of > 53 °C (Hölting and Coldewey, 2013; Röckel, 2014).

The calcite disseminated in the marble beds of Neusorg (11), however, does not show any resemblance with the REE patterns in Figs. 8 and 1c. Even if the Lu-contents are below detection limit, the La/Lu ratio is certainly > 1. Acidic fluids poor in complexing ligands, such as carbonates, evidently played a crucial role in the formation of blue fluorite. It is genetically unrelated to the marble host rocks and to the carbonate-bearing vein mineralization at Warmensteinach, but a unique very late-stage mineralization. Sánchez et al. (2010) reported REE contents of fluorite from the Berbes to Villabona carbonate-hosted fluorite deposits, Spain, which are comparatively low and which display a set of homogeneous hump-shaped graphs when normalized to PAAS with La/Lu ratios very well below 1. It may be denominated as a result of a “tertiary hydrothermal process” or “topomineralic effect”, caused by local redeposition of certain elements abnormally enriched in the granitic or gneissic host rocks. Irrespective of the derivation of fluids, the fluorite samples show more or less well expressed Ce anomalies (Fig. 8, Table 1). The negative Ce-anomaly in Lichtenberg-Issigau indicates oxidized conditions for hydrothermal alteration, whereas the Warmensteinach carbonate-fluorite vein-type deposits likely formed at more reduced conditions.

The PAAS-normalized REE pattern including its slightly negative Ce anomaly of the Holenbrunn carbonate is characteristic of marine carbonates and similar to the non-altered Wunsiedel Marble of the area

Table 2
REE contents of carbonate-hosted mineralization and REE-enriched lithologies referred to in the text given in ppm. REE element ratios and Eu and Ce anomalies are based on REE data normalized to PAAS. Numbers ("No") refer to the numbers used in Fig. 1b. REE data from Göpfersgrün and Sinatengrün have been taken in part from the literature and marked in italics (Hecht et al., 1999a).

Site	No	La	Ce	Pr	Nd	Sm	Eu	Gd	Tb	Dy	Ho	Er	Tm	Yb	Lu	La/Lu	La/Ce	Eu anomaly	Ce anomaly
Brandholz-Goldkronach	1	4.6	12.3	1.8	8.7	2.5	1.0	2.6	0.4	1.8	0.3	0.6	0.1	0.4	0.0	1.05	0.79	1.92	−0.32
Warmensteinach	2	1.7	7.5	1.6	10.4	7.7	2.2	7.5	1.3	6.7	1.2	3.5	0.6	6.2	1.1	0.02	0.47	1.34	−0.39
Holenbrunn	3	1.9	3.2	0.6	2.6	0.6	0.1	0.6	0.1	0.5	0.1	0.3	0.0	0.3	0.0	0.57	1.23	1.04	−0.46
Sinatengrün	4a	1.8	2.4	0.4	1.7	0.4	0.1	0.5	0.1	0.4	0.1	0.3	0.0	0.2	0.0	0.82	1.50	1.16	−0.46
Sinatengrün	4a	2.5	3.4	0.4	1.4	0.2	0.1	0.3	0.0	0.2	0.1	0.1	0.0	0.1	0.0	1.99	1.54	1.67	−0.43
Sinatengrün	4a	1.2	1.8	0.3	1.0	0.2	0.0	0.2	0.0	0.2	0.0	0.1	0.0	0.1	0.0	1.06	1.44	0.95	−0.45
Sinatengrün	4b	3.6	3.4	0.5	1.9	0.4	0.1	0.5	0.1	0.4	0.1	0.3	0.0	0.2	0.0	1.39	2.18	1.07	−0.53
Sinatengrün	4b	1.4	2.1	0.3	1.0	0.2	0.0	0.2	0.0	0.2	0.0	0.1	0.0	0.1	0.0	1.07	1.43	0.92	−0.43
Sinatengrün	4c	2.2	3.8	0.5	1.8	0.3	0.1	0.4	0.1	0.4	0.1	0.2	0.0	0.2	0.0	1.11	1.24	1.07	−0.37
Sinatengrün	4d	1.3	2.2	0.3	1.2	0.2	0.0	0.3	0.0	0.2	0.0	0.1	0.0	0.1	0.0	0.99	1.23	0.90	−0.39
Sinatengrün	4e	3.5	6.0	0.8	3.3	0.7	0.2	0.7	0.1	0.6	0.1	0.4	0.0	0.3	0.0	0.93	1.23	1.02	−0.39
Sinatengrün	4f	2.1	3.3	0.5	1.9	0.4	0.1	0.4	0.1	0.3	0.1	0.2	0.0	0.1	0.0	1.20	1.31	1.24	−0.41
Sinatengrün	4 g	13.4	11.4	5.2	23.4	5.3	1.2	5.2	0.7	3.9	0.8	2.1	0.3	1.5	0.2	0.69	2.45	1.10	−0.82
Sinatengrün	4 h	7.1	9.2	2.7	12.4	2.9	0.7	2.9	0.4	2.2	0.4	1.2	0.1	0.9	0.1	0.62	1.60	1.09	−0.63
Sinatengrün	4i	1.1	2.7	0.3	1.4	0.3	0.1	0.4	0.1	0.3	0.1	0.2	0.0	0.1	0.0	0.64	0.86	0.93	−0.30
Sinatengrün	4j	0.6	1.5	0.2	1.0	0.2	0.1	0.3	0.0	0.2	0.0	0.1	0.0	0.1	0.0	0.46	0.87	1.05	−0.36
Sinatengrün	4 k	0.7	1.2	0.2	0.8	0.2	0.0	0.2	0.0	0.2	0.0	0.1	0.0	0.1	0.0	0.59	1.28	1.03	−0.44
Göpfersgrün	5a	0.5	2.0	0.3	1.5	0.6	0.2	0.7	0.1	0.6	0.1	0.3	0.0	0.3	0.0	0.15	0.56	1.39	−0.29
Göpfersgrün	5a	1.9	5.1	0.7	2.7	0.6	0.2	0.7	0.1	0.5	0.1	0.3	0.0	0.2	0.0	0.68	0.78	1.40	−0.31
Göpfersgrün	5a	2.5	6.2	0.8	3.1	0.7	0.2	0.8	0.1	0.6	0.1	0.3	0.0	0.3	0.0	0.66	0.82	1.42	−0.30
Göpfersgrün	5b	6.8	20.2	2.9	11.3	2.7	1.0	3.3	0.4	2.2	0.4	1.0	0.1	0.6	0.1	0.99	0.70	1.62	−0.30
Göpfersgrün	5b	12.2	35.6	5.6	24.1	7.7	2.6	10.2	1.4	6.6	1.1	2.6	0.3	2.0	0.3	0.48	0.71	1.37	−0.33
Göpfersgrün	5b	13.1	34.9	5.1	20.9	6.5	2.4	8.5	1.2	5.5	0.9	2.1	0.3	1.5	0.2	0.66	0.78	1.53	−0.32
Göpfersgrün	5c	1.4	6.4	0.5	2.0	0.6	0.1	0.6	0.1	0.6	0.1	0.3	0.0	0.3	0.0	0.45	0.47	1.02	−0.07
Göpfersgrün	5c	10.0	23.7		10.7	3.0	0.7		1.2					6.7	1.1	0.10	0.87		
Göpfersgrün	5c	17.2	40.9		17.2	3.1	0.6		0.4					1.2	0.2	1.20	0.88		
Göpfersgrün	5c	68.7	219.1		99.9	15.0	8.3		4.8					7.8	0.9	0.85	0.65		
Göpfersgrün	5d	17.9	51.7		25.4	6.7	2.4		1.2					2.3	0.3	0.75	0.72		
Göpfersgrün	5d	54.3	126.5		49.4	9.6	4.5		2.0					3.5	0.4	1.59	0.89		
Göpfersgrün	5e	0.1	0.1		0.2	0.0	0.0	0.1	0.0					0.0	0.0	0.50	1.35	1.04	−0.73
Thiersheim	6	14.1	43.3	4.9	20.6	5.9	1.4	6.6	1.1	5.6	1.0	2.6	0.3	2.2	0.3	0.51	0.68	1.06	−0.23
Thiersheim	7	76.1	774.0	30.7	128.0	26.3	4.8	18.2	2.3	7.6	1.7	3.0	0.4	2.3	0.2	4.28	0.20	1.04	0.25
Stemmas	8	2.02	3.44		0.05	0.26	0.07		0.03					0.09	0.02	1.51	1.22		
Neusorg	11	0.6	1.5	0.2	0.7	0.1	0.0	0.2	0.0	0.1	0.0	0.1	0.0	0.1	0.0	0.66	0.82	0.94	−0.28
Wurlitz	14	8.1	19.4	2.7	12.1	2.8	0.7	2.9	0.4	1.8	0.3	0.8	0.1	0.4	0.1	1.75	0.87	1.19	−0.32

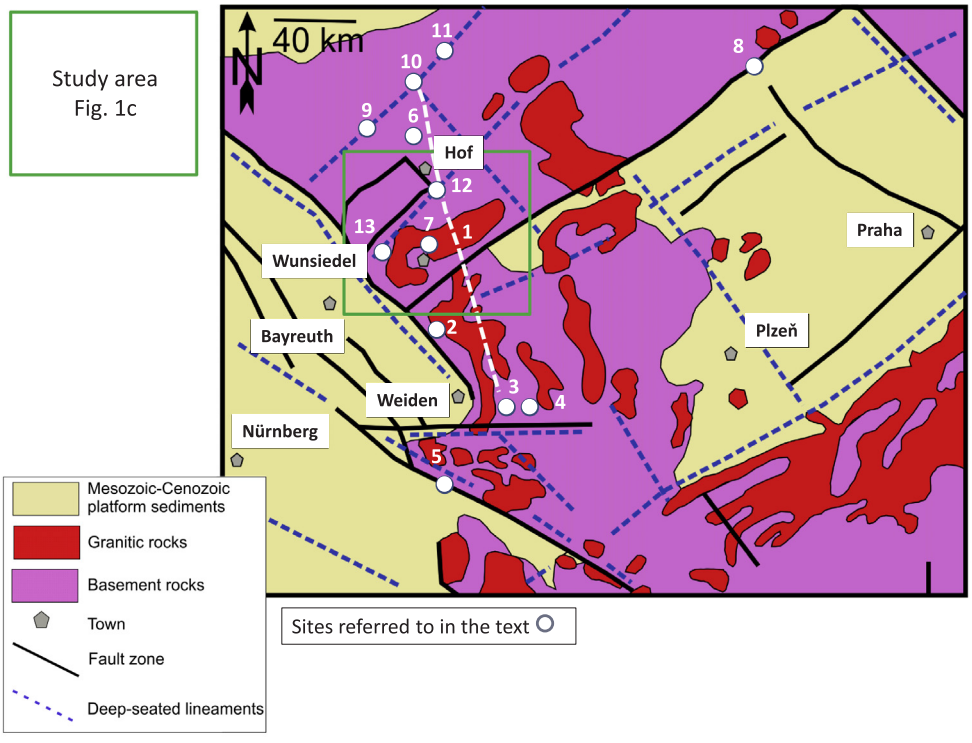

Fig. 9. Structural fragmentation at the western edge of the Bohemian Massif with sites referred to in the text and the position of the study area. Geology modified from the map of Teuscher and Weinelt (1972). 1: Central Fichtelgebirge Lineament (white stippled line), 2: Superdeep drill hole, 3: Pleystein (W), 4: Hagendorf-Pleystein pegmatite province, 5: Nabburg- (F-Ba), 6: Issigau-Lichtenberg (F-(Ba)), 7: Weißenstadt deep drill hole, 8: Teplice (F), 9: Wolfersgrün (Sb), 10: Schleiz (Sb), 11: Greiz (Sb), 12: Wurlitz: (Sb), 13: Brandholz-Goldkronach (Sb-Au).

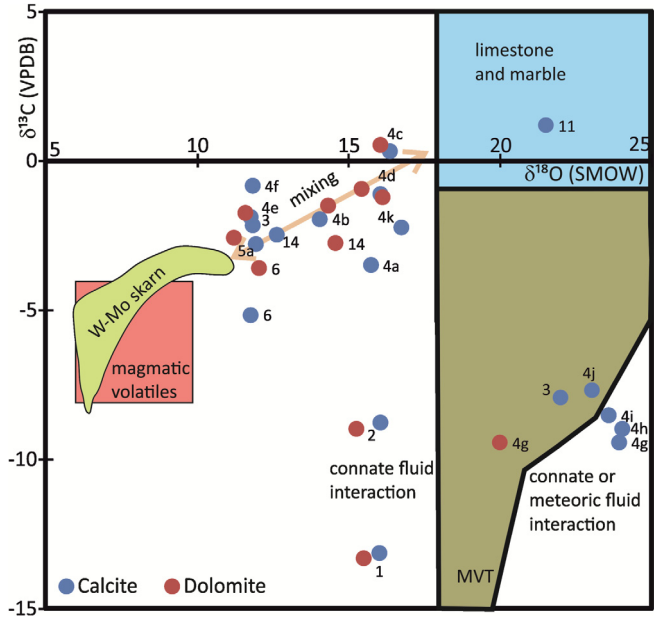

Fig. 10. Oxygen and carbon isotope data of calcite and dolomite samples of the carbonate mineralization on display in Fig. 1c. For localities see also Fig. 1c.

(Hecht et al., 1999a,b) (Fig. 1c). Alternatively, the Ce anomaly can be interpreted as a result of an oxidized nature of the hydrothermal fluids involved in the hydrothermal mineralization (Table 1). Most of the samples from Sinatengrün (4) record a negative Ce anomaly, whereas some samples show a positive Eu anomaly. These anomalies can be the result of relatively oxidized, high-temperature hydrothermal fluids altering the primary features of the marine carbonates. The pattern is similar to the non-altered Wunsiedel Marble of the area (Hecht et al., 1999a,b).

The variation in the Göpfersgrün (5) pattern is explained by analysis of various carbonate generations and variable interaction with hydrothermal fluids. Sample 5e reflects the REE signature of the unaltered Wunsiedel Marble, whereas the other patterns could be influenced by hydrothermal barite, fluorite and scheelite. However, Hecht et al. (1999a,b) describe a roof-shape for the REE pattern from separates of hydrothermal carbonate. The Thiersheim-I (6) pattern is explained by the flat pattern typical of the Wunsiedel Marble overprinted by hydrothermal fluids that are responsible for the roof-shaped REE patterns as represented in the hydrothermal carbonates elsewhere. Neusorg shows a flat PAAS-normalized REE pattern similar to the Wunsiedel Marble wall rock, which was slightly hydrothermally altered.

5.2. Carbon and oxygen isotopes - the hydrothermal system and the processes of concentration

The cross plot of Fig. 10 illustrates the various environments of formation and the hydrothermal systems as a function of the carbon and oxygen isotopes of calcite and dolomite.

The Brandholz-Goldkronach (1) calcite and dolomite samples differ from values typical of marble but overlap with typical values for metapelitic rocks (Hoefs, 2015). The carbonate mineralization developed likely from interaction with connate fluid, because $\delta^{18}O$ lies outside the typical field for metamorphic and magmatic fluids (Hoefs, 2015). Their data points overlap with those isotope ratios reported by Hecht et al. (1999a,b) for the vug-filling calcite$_3$, which postdates the massive dolomitization at the Göpfersgrün talc deposit. Since the carbonates formed in the Sb-Au veins, the stable isotope composition indicates connate fluids as a possible mineralizing fluid. The nearby Warmensteinach (2) shows a similar hydrothermal system as the afore-mentioned vein-type deposit although the carbonates formed at a different stage in barite-fluorite veins.

The calcite samples from Holenbrunn (3) differ significantly from typical marble or limestone composition and values previously reported from the area (Hecht et al., 1999a,b). The stable isotope data indicate hydrothermal alteration of the metacarbonates caused by mixing of two isotopically different hydrothermal fluids. Samples from Sinatengrün (4) similarly cluster in two different parts of the diagram (Fig. 10). A great deal of calcite and dolomite straddles the boundary between the territories typical of Mississippi Valley Type (MVT) deposits and connate water/ meteoric water interaction. Carbonates of these samples likely formed by interaction with a hydrothermal basin brine or an evolved meteoric water that interacted with the wall rocks before mineralization. The other group of samples clusters between typical W-Mo skarn/ magmatic volatiles and the field for unaltered limestone and marble. These data are interpreted as indicating fluid rock interaction between the host rock and a magmatic fluid during hydrothermal alteration. Sample 4b, dolomite from Sinatengrün, is the only sample from the current study that yields consistent temperature estimates from both, oxygen and carbon isotope fractionation between calcite and dolomite at approx. 550 °C. This indicates that the hydrothermal mineralization that involved magmatic fluids at Sinatengrün likely formed at these temperatures in the amphibolite facies. Göpfersgrün (5) isotope data overlap with data for dolomite$_3$ from Hecht et al. (1999a,b) and plot closely together with the latter group of samples from Sinatengrün (Fig. 10). Göpfersgrün is the only skarn deposit known from the area, supporting the interpretation based on the stable isotope data of fluid rock interaction involving a magmatic hydrothermal fluid at approx. 550 °C during mineralization. The dataset of Thiersheim and Wurlitz additionally follow closely the one of Göpfersgrün, indicating a similar hydrothermal system during mineralization (Fig. 10). Neusorg calcite is the only sample that plots within the characteristic field for marble and limestone compositions, and represents an only weakly altered case. Another option is that the hydrothermal fluid responsible for mineralization equilibrated isotopically with the host rock.

5.3. Major and minor elements – Tracking down the sedimentary and magmatic control of mineralization

5.3.1. Sedimentary control

The marble and calcsilicate beds mapped along the southern rim of the Fichtelgebirge Pluton are well-bedded, in places, and interbedded with mica schist, phyllite, and quartzite that can be traced over several tens of kilometers within Neoproterozoic through Cambrian units (Wurm, 1961) (Figs. 1c, 3). It is evident to treat those lithologies as metacarbonates and test and establish their original parent rocks by means of a litho-chemical facies analysis (Fig. 6). The dataset of the marble being normalized to pure marine limestone shows the best match. The increased Mg and Mn contents are explained by post-sedimentary dolomitization. The Mn/Sr ratio has been applied to elucidate the post-sedimentary alteration of the limestones (Derry et al., 1994; Kouchinsky et al., 2008; Ren et al., 2017). The ratios of the unmineralized marble horizons are as follows: Min: 0.0226, mean: 0.2470. max: 0.7451. They fall mostly in the territory below the critical level of 0.6 for calcareous rocks unaffected by diagenesis. Ratios not exceeding 2.0 signify sedimentary rocks of moderate diagenetic alteration. According to Dubois et al. (2015), elevated Mn contents are interpreted in terms of reducing conditions. These results may also be applied to the black shales intercalated among the calcareous rocks. The calcsilicates normalized to impure marine limestone provide a similar picture as the marble and attest to similar depositional environments which only differ from each other with regard to the detrital influx (Fig. 6). Both lithologies have elevated P contents similar to the stratabound Fe deposits (Fig. 7, Table 3). Phosphate is genetically related to the host-rock sediments and its contents were left unaffected, when Fe accumulated in the calcareous rocks. There are transitions from siliciclastic- to carbonate-hosted phosphorite deposits to be found all across the globe

Table 3
Chemical composition of stratabound and vein-type Fe ore mineralization.

	No	Fe_2O_3	P_2O_5	MnO	As	Cu	Ni	Pb	W	Zn	Ba	Co	Cr	Sc	V	Type
		wt%	wt%	wt%	ppm	ppm	ppm	ppm	ppm	ppm	ppm	ppm	ppm	ppm	ppm	
Arzberg	9	64.81	0.63	4.5	15	38	52	< 5	< 5	< 5	61	38	52	10	45	Stratabound
Arzberg	9	60.18	0.63	1.16	26	56	43	13	< 5	< 5	63	51	23	6	41	Stratabound
Tröstau	13	53.41	0.84	9.81	28	< 5	73	18	< 5	114	232	0	32	9	60	Stratabound
Tröstau	13	69.67	1.16	0.51	47	< 5	132	27	< 5	1822	87	0	43	11	80	Stratabound
Aign	10	63.56	0.57	0.28	133	574	30	< 5	< 5	47	42	0	9	12	58	Stratabound
Schanzberg	2	58.29	0.03	5.19	29	< 5	48	< 5	< 5	< 5	322	0	0	10	36	Vein-type
Mittelberg	2	61.77	0.01	1.73	330	251	29	< 5	< 5	< 5	6	0	11	0	42	Vein-type
Mittelberg	2	46.2	0.06	3.41	15	41	15	< 5	< 5	17	0	0	0	0	43	Vein-type

(Dill and Kantor, 1997).

5.3.2. Structural control

The Variscan basement block of the Bohemian Massif was fragmented and differentially uplifted after cessation of the Variscan orogeny (Fig. 9). One of the deep-seated fault zones, the Central Fichtelgebirge Lineament, strikes NNW-SSE and intersects a wide variety of crystalline rocks, from ultrabasic magmatic rocks all the way down southward to the granites and pegmatites (Figs. 1c, 9 see white stippled line running from site No 10 to site No 3). The major elements of the granite-hosted episyenite form a circular pattern terminated by the "red-ring" in the spider diagram (Figs. 5 and 7). Only K exceeds this standard, a fact accounted for by the intense muscovite-calcite alteration taking in the vuggy episyenite. Among the trace elements, Rb and Pb underscore this type of alteration, while the U anomaly is due to the main ore minerals uraninite, coffinite and brannerite. The stratabound Fe and vein-type deposits are both enriched in siderite, whereas the remaining elements reflect the presence or absence of dolomite. The talc deposits are enriched in Si and Mg, while being depleted in the remaining elements. Top-down, the spider diagrams reveal a decreasing subcrustal or mantle impact on the mineralizing fluids along a deep-seated structure zone common to all of these mineral associations (Fig. 1c, 3, 9–1).

5.4. The evolution of carbonate-related metallic and non-metallic mineral assemblages as a function of temperature

The majority of the hydrothermal mineral assemblages contains Ca-bearing silicates and allows for a determination of the formation temperature (Table 4). The T interval for hydrothermal alteration covers the temperature range from 745 °C down to 53 °C.

5.4.1. Pegmatite skarn

In the study area, pegmatite skarn has only been identified at Göpfersgrün, where it is highlighted by the presence of Be minerals (Tables 1 and 4). Apart from that site, there are several locations at the western edge of the Bohemian Massif where pegmatites are associated with marble, calcsilicate rocks and skarn deposits (Figs. 9-3, 4). The pegmatite at Vlastějovice near Zruč nad Sázavou, Czech Republic, has Fe-skarn as host rock besides biotite-sillimanite gneiss, amphibolite, quartzite and marble (Novák and Hyršl, 1992; Žáček et al., 2003; Ackerman et al., 2007). Near Wimhof south of Göpfersgrün, anatase, titanite, ilmenorutile, apatite, beryl, titanite, garnet, andalusite, tourmaline and magnetite were found. Only in the scheelite-skarn deposit west of the Hagendorf-Pleystein Pegmatite Province known for its abundant Li, Nb/Ta and Be minerals, wollastonite was found in the calcsilicate host rock accompanied by grossular (hessonite), diopside-hedenbergite, clinozoisite s.s.s., vesuvianite (Dill, 2015b). Wollastonite formed at a site approx. 10 km S of the most proximal highly-fractionated granite and < 1 km away from the center of the pegmatite in a wollastonite-bearing calcsilicate skarn. The older and the younger granites rarely show hornfels around them. If present at all, the intrusive rocks developed contact-metamorphic rocks indicative of the albite-epidote hornfels facies according to Winkler (1976), which attests to a temperature interval of approximately 400–500 °C. The process leading to wollastonite formation, when CaO and SiO_2 react, is a classical one and has already been discussed by V.M Goldschmidt so that it is quoted in almost each textbook of petrology (Bucher and Grapes, 2011). Petrographic observations in the field indicate that the X_{CO2} was rather high and a temperature of 600 °C existed at a depth of 2 km, corresponding to a pressure of 0.5 kbar due to the widespread occurrence of calcsilicates. At 4 km depth (1 kbar) temperatures of between 650 and 670 °C are required to produce wollastonite. Whatever temperature of formation has been invoked, the temperature anomaly cannot be accounted for by the older or younger granites. At Göpfersgrün, Be was mobilized as thin aplite veins intruded the metacarbonate at a temperature between 430 °C and 570 °C, marked by the presence of grossular. This area is a LP/HT "hot spot" like the hydrothermal alteration linked to the largest pegmatite mineralization in Central Europe, the Hagendorf-Pleystein Pegmatite Province (Dill, 2015b). The stable isotope data of hydrothermal carbonate plot along a mixing line between "skarn-type" mineralization or magmatic volatiles and limestone or marble (Fig. 10). This indicates that the hydrothermal alteration and mineralization is best explained by mixing of magmatic hydrothermal fluids and fluids that equilibrated with the host rock. Such a scenario also explains the temperature anomaly by the migration of hot magmatic volatiles, exceeding the temperature of the wall rocks that mixed with colder fluids at sites with high (structural) permeability.

Both, the whole rock REE chemistry and the stable isotope data for Göpfersgrün are similar to $dolomite_3$ of Hecht et al. (1999a,b). This dolomite generation belongs to the late-stage hydrothermal assemblage, which formed at 400–250 °C. The whole rock REE data and mineral separate isotope data, thus, record the late-stage hydrothermal overprint. This is well known for stable C- and O-isotopes in metamorphic, magmatic and complex hydrothermal systems, where coexisting minerals record isotopic disequilibrium due to fluid-assisted isotopic exchange between the phases during cooling (e.g., Rumble, 1982; Krylov, 1985; Valley, 1986; Chacko, 1990; Kolb et al., 2000; Hoefs, 2015).

The extraordinary high T values discussed in this section cannot be genetically explained by the Late Variscan granites and stress the presence of a subcrustal heat source. It has only been spotted at the southernmost end of the Central Fichtelgebirge Lineament in the Oberpfalz, which likely formed the pathway for high-temperature hydrothermal fluids with a magmatic stable isotope signature (Figs. 9 and 10).

The calcsilicate-bearing metacarbonate rocks underneath the rare-element pegmatites and pegmatoids have to be denominated as Ca metasomatites which have been derived from the surrounding host metapelites. This is proven by lithochemical marker elements such as W and Ca and the presence of wollastonite can explain why a great many rare-element pegmatitic bodies are encased by metabasic rocks as exemplified by pegmatite deposits in Canada, Australia, Sweden, Norway

Table 4
Formation of calcsilicate-minerals as a function of the temperature of formation in the different carbonate-related mineral associations with their age of formation, their structural characteristics and the ore type. The color shades are used to group the corresponding facies regimes: high T (red), medium T (purple), low T (blue), very low T (1) (brown), very low T (2) (yellow).

Ca-Mg-(Fe) marker silicates	Stages	Wollastonite	Vesuvianite	Diopside	Grossular (andradite)	Clinozoisite (epidote)	Tremolite (actinolite)	Prehnite	Laumontite	Stilbite-heulandite	Age	Structure	Stratabound	Thrustbound	Collision-related	Related to deep-seated fault zones
Bi-Au-As-Sb veins	1						< 450°C	≅ 300°C	< 260°C	< 200°C	Carboniferous	N-S, NNE-SSW, NE-SW rarely NW-SE		+		
Sb-Hg-Mo veins	1						< 440°C	≤ 300°C Brand-holz	150 – 220 °C Wurlitz		Carboniferous Permian	NNW-SSE		+		+
Pegmatite and pegmatite skarn	2	600 - 670°C	400 - 600°C	430 - 570°C	430 - 570°						Carboniferous Permian	NNW-SSE /NNE-SSW rarely NW-SE		+	(+)	+
W skarn	2		400 - 600°C	430 - 570°C	430 - 570°	400 - 530°C					Early Permian	near NNW-SSE			+	
Fe carbonate replacement	3						100 (?) – 470°C				Protore: Early Paleozoic, ore: Permian	NNW-SSE / NNE-SSW	(+)			+
Talc replacement	4					400 - 530°C	350 - 450°C				Permian	NNW-SSE				+
Halloysite-kaolinite replacement	4							< 400°C	<400° C		Permian	NNW-SSE				+
U-bearing episyenites	4							53 - 400°C	<400° C	230-260°C	Permian	NNW-SSE				+
Ni-Co veinlets	5					330-550°C MP	330-550°C MP	130 - 280°C LP	130 - 280°C LP	130 - 280°C LP	?	n.d.				+
Pb-Cu-Zn-F veins /veinlets	5					330-550°C MP	330-550°C MP	330-550°C LP	130 - 280°C LP	130 - 280°C LP	?	NW-SE				+
F-Ba veins	5									< 200°C	Permian to Late Cretaceous (Neogene?)	NW-SE disseminated				+

Thrustbound (metamorphogenic) = lower crustal impact

Collisional = lower crustal impact

Related to deep-seated fault zones = subcrustal impact

Stratabound = crustal impact (low metal concentration / "protore")

n.d. = not determined

MP = medium pressure

LP = low pressure

(+) = subordinate process of concentration

+ = Major process of concentration

and Austria (Schneiderhöhn, 1961; Partington et al., 1995; Černý et al., 1996; Selway et al., 2000; Van Lichtervelde et al., 2006). The study focusing on this peculiar coupling of basic restite and mobilizate has not yet been fully investigated.

5.4.2. Scheelite skarn

Scheelite mineralization is confined to a few places in marble and calcsilicate rocks, where W minerals are invariably associated with diopside, grossular, clinozoisite and vesuvianite (Tables 1 and 4). The latter calcsilicate mineral is diagnostic for scheelite mineralization in

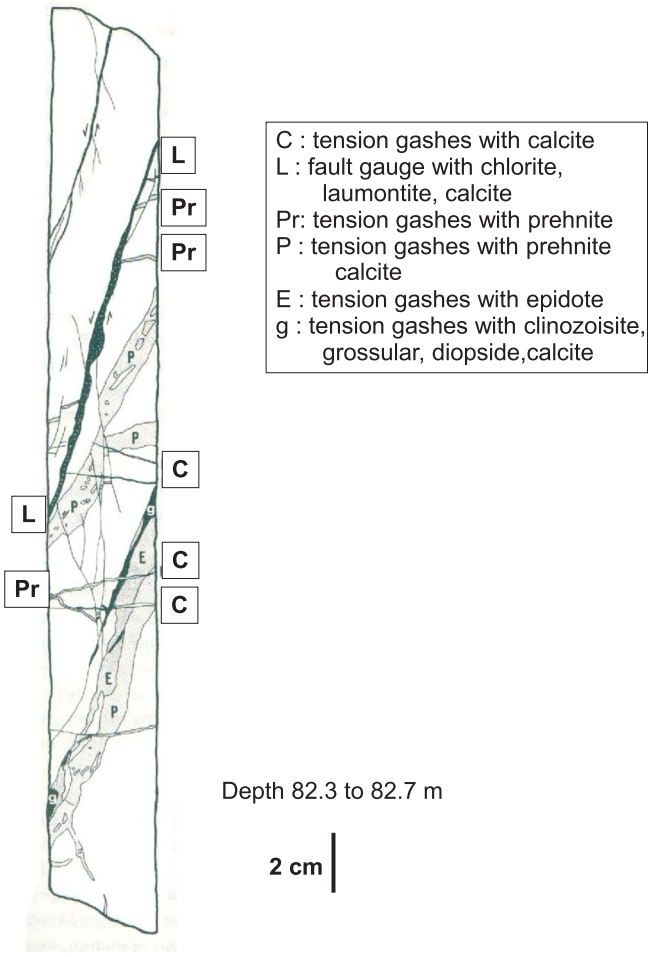

Fig. 11. Alteration in calcsilicate amphibolite recorded by Zulauf (1990) from the Zone of Erbendorf-Vohenstrauß.

the periphery of granites. While the pegmatite skarn is found in the so-called high-temperature facies equivalent to the K-feldspar-cordierite hornfels facies, diopside, grossular and vesuvianite are representative of the medium-temperature facies also named hornblende hornfels facies (Table 4) (Shoji, 1975; Ahmed-Said and Leake, 1996; Patel, 2007). Vesuvianite is a silicate, which is stable over a wide temperature range and very sensitive to the H_2O and CO_2 contents in the system. It converts together with clinozoisite/epidote, or tremolite and quartz into grossular, diopside and water and can be used in this case as a critical marker mineral for the boundary between the medium- and low-temperature contact metamorphic facies (also called albite-epidote hornfels facies). There is no coherent zone around the older or younger granites composed of these calcsilicate minerals. They occur isolated or as veinlets (Zulauf, 1990) (Fig. 11). This LP/MT to LT calcsilicate mineralization is the oldest structurally controlled hydrothermal mineralization in subvertical tension gashes and grading in unzoned skarn replacement bodies hosting scheelite.

5.4.3. Talc replacement deposits

Talc replacement deposits occur within the dolomitized marble and in ultrabasic igneous rocks restricted to zones where the host lithology is intersected by fault zones. In pure marbles, the talc deposits are associated with chlorite and dolomite, whereas in ultrabasic rocks, tremolite-actinolite s.s.s. forms the hydrothermal alteration. Magnesium has been derived from the Mg-enriched host rocks. The Mg metasomatic processes affected also the Mg-poor wall rocks, but they fell short of reaching the talc level and mainly formed chlorite instead (Table 1). The subvertical tension gashes neither contain talc and tremolite nor

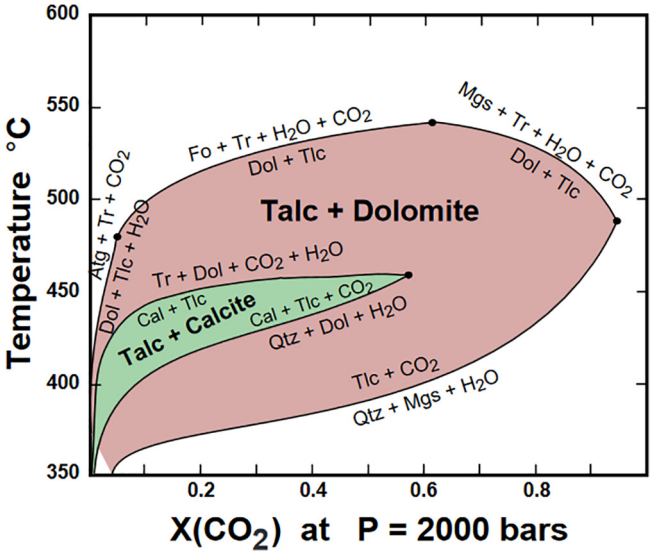

Fig. 12. Temperature-pressure phase diagram to display the stability fields of talc-dolomite system for different X_{CO2} (Brady et al., 1998).

dolomite (Fig. 11). The talc deposits resemble those described by Anderson et al. (1990) from the Ruby Range in SW Montana, USA. The metasomatic replacement process is, however, placed at a higher temperature as being calculated for 2 kbar at different X_{CO2}. Hecht et al. (1999a,b) concluded that the main talc mineralization resulted from decarbonation reactions at low X_{CO2} and temperatures between 250 °C and 400 °C. Brady et al. (1998) published a phase diagram at 2 kbar for different X_{CO2} (Fig. 12). Even at very low X_{CO2}, the lower temperature limit should be placed around 350–370 °C and the upper limit 450 °C. A $X_{CO2} = 0$ is unrealistic in a thick marble horizon. Formation of talc lies within a temperature interval where vesuvianite, clinozoisite and tremolite are stable, but they are not directly involved in the replacement process of talc and held to be marker minerals for the critical zone between Sinatengrün and Thiersheim. Talcitization is the LP/LT part of a LP/MT-LT metamorphic –metasomatic catena of processes.

Talc is restricted in the study area to the central facies, where replacement deposits are most widespread near the intersection of the marble beds and the rhyolite dykes (Fig. 3a). The location of talc mineralization is, however, unrelated to any of the granite members of the older and younger granites of the Fichtelgebirge Pluton.

5.4.4. Fe carbonate replacement deposits

Tremolite is the only calcsilicate mineral, which co-exists with a series of Fe-Mn carbonate minerals and the ubiquitous dolomite in the Arzberg Mining Area. There is a stratabound Fe protore as attested to by the pre-kinematic siderite at Tröstau, but the main Fe concentration accountable for the minable Fe accumulation, is that of a replacement process controlled by fault zones cross-cutting the marble (Figs. 3a and b, 6, Table 3). They may be assigned to the group of hydrothermal Fe replacement (metasomatic) deposits occurring in limestone with ankerite, siderite and Fe dolomite accompanied, in places, by base metal sulfides, hematite and barite. No contact-metasomatic or –metamorphic aureole or skarn is recognized. Examples of this type of Fe deposits are known from Erzberg, Radmer, in Austria; from Bilbao, Spain, Westcumberland and Lancashire, Great Britain, Kremikovtsi, Bulgaria, Ljubija, Bosnia-Herzegovina, Nižná Slaná, Dobšiná – Mlynky area, Slovakia, Rudabánya, Hungary, Lake Como Area, Caffaro Valley, Italy, Warda, Jordan and in part of the Rude deposit, Croatia (Dill 2010). Some of them formed on top of rising salt diapirs such as at Ouenza, Algeria, and Jerissa, Tunisia (Bechtel et al., 1996). Brines expelled from the evaporites reacted with the wall rocks during early diagenesis becoming acidic and reduced, and thus allowing dissolution and transport

of Fe and other cations. Ore-bearing solutions were channeled towards the apical parts of diapirs, where they deposited their solute by metasomatic processes in fractured roof carbonates. The metasomatic processes involve deep hydrothermal fluids heated by basic magmas, as suggested by Huang et al. (2015). The temperature of formation spreads a wide T interval starting from 470 °C, which is similar to the temperature calculated for ankerite and siderite of the Steierische Erzberg and Radmer in Austria by Beran (1979): 450 °C/2–3 kbar. The lowermost T values can only be assumed from collomorphous siderite (≅100 °C). It is a matter of discussion whether the conditions leading to the consanguineous sparry siderite and magnesite deposits of the Eastern Alps, forming the most proximal and largest mineral province of its kind, are comparable with those in the study area.

The formation of epigenetic/metasomatic siderite in the Alpine Mts. Chain is related to Permoscythian rifting and the circulation of brine-derived fluids. Arguments for this model are based on field observations and the chemistry of fluid inclusions (Ebner et al., 2000). The age of formation of the afore-mentioned Fe deposits spans the interval Permian-Triassic. Highly fractionated hypersaline fluids exhibiting all the hallmarks of residual bittern brines were mobilized either by magmatic/metamorphic processes in the underlying crystalline units or by the superimposed sedimentary upload of the Triassic platform carbonates. Initially, these residual, bittern brines were completely free of Fe and rich in Mg suitable for the formation of magnesite. Deeper and more extensive circulation of these fluids and their interaction with the host-rock, resulted in the uptake of Fe and the formation of siderite. Although, there are some striking differences with regard to the geodynamic setting between the Central European Variscides and the Alpine Orogen, there are also some similarities applicable to the sites under current investigation. Mineralization caused by Mg metasomatism close to the SSE-striking master fault system in the environs of Göpfersgrün and Thiersheim is substituted for by a marginal facies on both sides of the fault characterized by iron metasomatism, which may be interpreted by means of convective cells gradually affecting deeper parts of the basement.

5.4.5. Calcareous U-bearing episyenite

The vuggy and highly permeable episyenites formed a shallow crustal level, with fluid inclusion data indicating entrapment under pressure conditions of < 1.0 kbar (Borges et al. 2009). The temperature interval during which episyenitization took place is difficult to constrain as demonstrated by the following examples. Borges et al. (2009) claimed fluid temperatures in the range 400–100 °C responsible for all dissolution processes. Recio et al. (1997) assumed a high-temperature (300–450 °C) late-magmatic deuteric fluid to have created this porous lithology. Dosbaba and Novák (2012) published a temperature range of 100 °C–300 °C and a pressure range of ~0.5–1.0 kbar, under high alkali activity and low tectonic stress. In the classical studies of Leroy (1978), an average temperature of 300 °C at 0.41 kbar was estimated based on fluid inclusion studies. The latter physical parameter at 1.25 kbar is representative of a depth of episyenitization around 4700 m. The monotonous mineralization of U oxides, U titanates and leucoxene, and carbonate in the episyenite, which were investigated during the 1980s, formed at temperatures < 400 °C, for which no distinctive mineral assemblages are observed. The zeolite-bearing episyenite hosting heulandite and stilbite record an upper temperature limit of 200 °C and a maximum pressure of 2 kbar (Table 4) (Bucher and Grapes, 2011). With regard to laumontite, PT conditions are constrained below 230–260 °C and 3 kbar. The zeolites disappear in the presence of fluids containing appreciable amounts of CO_2. That is why carbonate-bearing episyenite "productive" with respect to U never co-exists with "barren" zeolite-bearing episyenite as in the study area. The stability field of prehnite is difficult to confine and lies between 100 and 300 °C (Bucher and Grapes, 2011).

Göpfersgrün and Wurlitz represent the mineralization at the opposite ends of the Central Fichtelgebirge Lineament. Their dataset manifests that their late-stage hydrothermal overprint was a regional feature and the hydrothermal fluids had a relatively uniform composition with respect to REE and C- and O-isotopes. Episyenitzation is a post-granitic hydrothermal process, which operated only in the central facies. Corresponding to the overall close resemblance of the carbonate mineralization at Wurlitz and Hebanz, a subcrustal process is suggested to be responsible for this intragranitic carbonate mineralization in the episyenites.

5.4.6. Hypogene kaolinization

Kaolin is a common raw material concentrated on top of the granite and its immediate surroundings, attaining economic grade mainly as a product of supergene conditions (Dill, 2016). Hypogene kaolinitization in and around granites is restricted in the NE-Bavarian to a few places, which stand out by the presence of kaolinite and halloysite and as halloysite-only deposits (Table 1). Kaolinite group phyllosilicates are characterized by a rather sharp upper limit of their temperature of formation of 390 ± 10 °C at a pressure of 2 kbar. Exceeding that temperature provokes kaolinite-group minerals to convert into pyrophyllite, which has not been identified in any of the deposits under consideration. An abnormally high structurally controlled content of LREE bound to phosphate is interpreted as hypogene alteration as is the case for halloysite in the apical parts of the Pleystein pegmatite.

The REE pattern of samples from the Thiersheim deposit resembles typical patterns for halloysite and does not reflect the high LREE contents otherwise reported. The hypogene kaolinitization leading to the rare modification halloysite is minero-stratigraphically equivalent to the concentration of talc in the metacarbonates (Table 4) (Dill, 2016). It differs, however, by its host rock lithology, which is siliceous, and by the mineralizing fluids, which are acidic in comparison to the talc mineralization.

5.4.7. Bismuth-gold-arsenic mineralization

No precise temperature data for this rare type of mineralization can be given. Gold-arsenic mineralization only formed in the distal zone outside the granite pluton. Reutel (1992), who studied the fluid inclusions of some of the vein mineral assemblages, described the mineralizing fluid as highly saline due to boiling at 0.8 kbar and 300 °C. Stilbite was identified at Goldkronach and attests to a late-stage mineralization at a temperature of < 200 °C.

The arsenopyrite mineralization that is bound to low-grade metamorphic marble manifested by the marker mineral tremolite is markedly different from the carbonate-bearing vein-type mineralization and devoid of gold (Table 4). Friedrich et al. (1991) reported a mineral assemblage consisting of arsenopyrite-chalcopyrite and little loellingite. The authors published a maximum formation temperature of 449 ± 36 °C. Arsenic- and Au mineralization is in this site part of the HT mineralization of the metamorphic wall rocks. The whole rock REE pattern does not show any influence of a hydrothermal overprint and resembles the Wunsiedel Marble.

5.4.8. Antimony-mercury-molybdenum mineralization

Excluding Brandholz-Goldkronach, Sb minerals are present only in subordinate amounts near deep-seated fault zones and are thereby only of genetic relevance (Table 1). Stibnite tends to precipitate at lower temperatures and lower pH than sulfosalts (Krupp, 1988). Increasing alkalinity common to veins mineralized with siderite as major gangue mineral favors the development of complexes like $Sb_2S_4^-$ and hence the precipitation of Sb sulfosalts such as at Brandholz-Goldkronach, whereas veins with only little siderite such as Göpfersgrün or Wurlitz bear stibnite-only mineral associations (Table 4). In the immediate surroundings of the Fichtelgebirge Pluton, Hg has only been found to be accommodated in the lattice of fahlore (tetrahedrite). Further south, Hg is also encountered as discrete minerals of cinnabarite along shear zones devoid as to carbonate gangue but abundant in metamorphic bitumen (impsonite). Epi- to kataimpsonite, a series of metamorphic

bitumen, forms between 100 °C and 300 °C and has been found in the vein-type mineralization at Mähring, Germany (Dill and Weiser, 1981). This temperature range can also be applied to the molybdenite mineralization, which is associated with the same type of metamorphic bitumen. With regard to the temperature of stibnite formation, the fluid inclusion data recorded by Reutel (1992) – highly saline fluids achieving a temperature at 0.8 kbar and 300 °C - are valid also for the stibnite-sulfosalt veins. In the Masawa orogenic gold deposit, quartz-stibnite-gold veins formed at a temperature range of 220 °C–310 °C, quartz-pyrite-arsenopyrite-gold veins between 250 °C and 315 °C/ 1.00–1.65 kbar. Only the barren quartz-molybdenite veins exceed these T intervals considerably and form in the T range 320 °C–400 °C (Jenkin et al., 2015). The stibnite ore deposits of the French Paleozoic basement developed subsequently to an Fe-As assemblage at 300–400 °C and 0.5–0.8 kbar between 150 °C and 270 °C at around 0.1 kbar (Munoz et al., 1992). The current investigation benefits from a fluid inclusion study published only recently on the antimoniferous vein-type mineralization of the Berga Antiform, Germany (Krolop et al., 2018). The sulfide-sulfosalt-quartz-carbonate mineralization is arranged along the fold axis of the afore-mentioned host anticline. The early Sb-bearing quartz mineralization is attributed to the Late Variscan mesothermal gold-antimony vein-type deposits scattered across the Central European Variscides, a member of which is found in the study area at Brandholz-Goldkronach and induced by the late stage Variscan deformation (Table 1) (Dill 1985b, Dill et al., 2008b). The younger Sb mineralization accompanied by carbonate gangue minerals, however, is post-kinematic and bound to the Franconian Line. The missing link between the mineral assemblages under study and those at the Berga Antiform (Wolfersgrün, Schleiz, Greiz) is the Wurlitz Sb mineralization (Fig. 9). Krolop et al. (2018) report the following physical-chemical data, which can be applied to the carbonate-bearing vein-type Sb-Hg-Mo association: Stage II: T = 220–226 °C (H_2O-CO_2-NaCl fluid, with 1–2.7 wt% $NaCl_{eq.}$), stage III T = ≥146 °C (H_2O-NaCl-$CaCl_2$ fluid, with < 8.1 wt% $NaCl_{eq.}$), stage: IV T ~ 220 °C (H_2O-NaCl-$CaCl_2$ fluid with > 20 wt% $NaCl_{eq.}$) and homogenization into the liquid phase at around 120 °C. Fluid inclusion data indicate P-T-conditions at the onset of mineralization at around 220 °C at 0.70–0.75 kbar (fluid pressure). Ore stages III and IV reflect a mixing of different fluids (see also Fig. 10). The mineral association discussed in Sections 5.4.7 and 5.4.8 mark the transition from intracrustal synkinematic Au-As-Sb mineralization bound to deep-seated thrust planes to postkinematic subcrustal Sb-Hg-Mo mineralization which is based on the temperature of formation, the structural positioning, and marker minerals as well as elements.

5.4.9. Nickel-cobalt and lead-zinc- copper mineralization

Nickel-cobalt accumulation is restricted in the carbonate-bearing mineral associations to the pentlandite-pyrrhotite group (34.2 wt% Co + Ni) and bravoite (14.6 wt% Co + Ni). Excluding rare millerite (64.7 wt% Co + Ni) at Wurlitz, no discrete Ni-Co minerals occur in the study area. All of the afore-mentioned sulfides are present in rather scant amounts. Their existence is in stark contrast to what has been described from the super-deep borehole (9100 m) immediately south of the study area by Friedrich et al. (1988, 1991)). The authors recorded a highly varied Ni-Co mineral association disseminated in the paragneiss and metabasic rocks: violarite (36.9 wt% Co + Ni), Ni siegenite (50.9 wt% Co + Ni), Co siegenite (51 wt% Co + Ni), polydymite (51.9 wt% Co + Ni), Ag pentlandite (18.2 wt% Co + Ni), Co pentlandite (41.7 wt% Co + Ni), gersdorffite (34.2 wt% Co + Ni), cobaltite (10.7 wt% Co + Ni).

Largely, the deep-seated Ni-Co mineral association is more abundant in Ni + Co, more varied and, demonstrated by the Ni-Co arsenides, lower in sulfur. The authors found twinned chalcopyrite, which is indicative of a phase transformation from the cubic HT chalcopyrite into the tetragonal LT chalcopyrite at 550 °C. Silver-bearing pentlandite segregated at a temperature between 330° and 455 °C from chalcopyrite. Normal pentlandite re-equilibrated at temperatures below 135 °C. The disseminated Ni-Co-Cu-Zn mineralization developed under MP metamorphic conditions of 5.5 ± 1.5 kbar at temperatures of as much as 600 ± 50 °C.

In drill holes of the pre-well-site studies, marble horizons are rare and only in one hole metacarbonate was transected at shallow depth of 208 m. It hosts a sphalerite-galena assemblage, which is identical to the mineralization between 1500 and 2500 m drill depth along shear zones and the mineralization in the marble under study (Friedrich et al., 1989). Corrected to a pressure of 1 kbar, the fluid inclusion data reported by Reutel et al. (1989) provide a temperature interval for the above LP mineral association in the T range 260–280 °C, which can also be applied to the shallow carbonate-hosted mineralization studied at outcrop (Tables 1 and 4).

5.4.10. Fluorite-barite mineralization

The Warmensteinach vein system with fluorite and barite at the western margin of the study area is located where the pluton dips underneath the metamorphic country rocks (Fig. 1c, Table 1). The temperature of formation of the vein-type deposits is deduced from the studies by Behr et al. (1987a,b), who focused their fluid inclusion studies on fluorite and obtained a formation temperature of < 200 °C. A similar study for the disseminated purple fluorite in marble is missing (Fig. 4d). More detailed information of the physical-chemical regime is obtained from the REE distribution in carbonate minerals and fluorite (Section 5.1).

The LREE of the Warmensteinach vein are depleted with respect to PAAS, whereas the MREE and HREE appear not to be affected. The fluid is a gneissic leachate as demonstrated by the REE pattern in Fig. 8. The pattern is explained by the fluorite mineralization. The stable isotope data of calcite and dolomite are different to any values previously reported (Hecht et al., 1999a,b). They are likely caused by the interaction with connate fluids.

5.5. Synopsis – The evolution of the carbonate-hosted and -related mineralization

According to the subdivision proposed by Dill et al. (2008b) for the ore and industrial mineral deposits in Central Europe, the mineral deposits and occurrences under consideration are attributed to the stratabound, thrustbound and fold-related metamorphogenic deposits, collision-related deposits and deposits related to the Franconian Line (Table 4, Fig. 9). The evolution of the various ore type has been illustrated in Fig. 13.

5.5.1. Thrustbound mineralization

The onset of thrustbound mineralization corresponds to the latest stages of the Variscan dynamo-metamorphic alteration during the Devonian-Carboniferous period (Table 4-stage 1). The state of alteration attained very-low to low grade metamorphic conditions and the mineralized structures are aligned predominantly in NE to NNE direction parallel to the axis of the major anticlines. Of the element assemblages emplaced along these structures, only Sb, Hg and Mo underwent a post-granitic remobilization along deep-seated fault zones during the Permian, which intersect the anticline axis at obtuse angle (Table 4-stage 1, Fig. 9). Mercury is not only widespread in Late Paleozoic sediment- and volcanic-hosted deposits in Central Europe but its gaseous emanations expelled from magmatic sources are also considered as culprit for the Late Paleozoic Mass Extinction and thereby cast in the role of a time bound marker element (Bond and Wignall, 2014; Grasby et al., 2016). Excluding the pegmatite deposits, none of the remaining mineralization is dated. The pegmatite deposits developed in the interval between 317 ± 3 Ma and 299.6 ± 1.9 Ma or in chrono-stratigraphic terms during the Late Carboniferous based on K/Ar, Ar/Ar data of mica and U/Pb data obtained from studies of columbite (Glodny et al., 1995; Dill et al., 2008b). Pegmatitic rocks cover the entire spectrum of emplacement processes from metamorphogenic, through

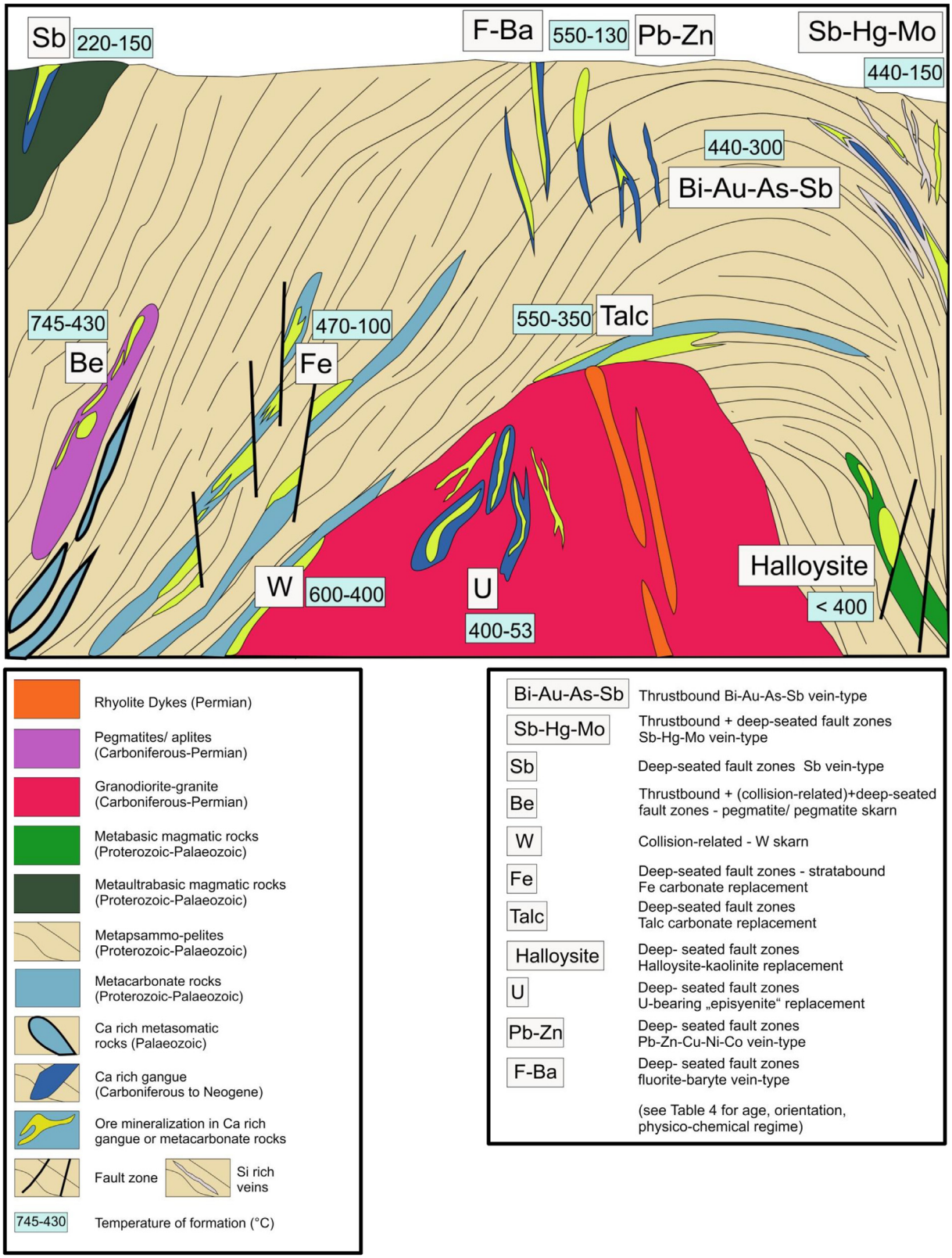

Fig. 13. A cartoon (not to scale) to show the evolution of carbonate-related metallic and non-metallic mineralization within the granites, proper, and their country rocks. The age of formation is getting younger from thrustbound through mineralization related to deep-seated lineamentary fault zones.

granite-related to structurally controlled by fault zones parallel to the Franconian Line (Dill, 2015a,b) (Table 4-stage1 + 2).

5.5.2. Collision-related mineralization

Collision-related mineralization is almost synonymous with a strong genetic correlation with the granites arranged in NW-SE direction along the Fichtelgebirge-Erzgebirge Anticline in the northern part and

arranged in NNW-SSE direction in the southern part of the study area more or less parallel to the general strike of the deep-seated lineamentary fault zones (Figs. 1c, 9). Despite their wide occurrence, the granitic influence on the carbonate-bearing mineralization is remarkably limited and confined to the Sn-W skarn mineralization only (Table 4). The W skarn mineralization is younger than the older granite and based upon the chemical similarities genetically akin to the so-called tin granite G 4, which is chronologically constrained at 290 ± 4 Ma, an Early Permian age of formation (Besang et al., 1976). The overall influence on the emplacement of pegmatites exerted by granitic magmas is negligible on temperature grounds. During stage 2, NNW-NW became the predominating orientation of the younger carbonate-bearing mineralization (Table 4).

5.5.3. Stratabound low metal concentration and replacement deposits related to deep-seated lineamentary fault zones

The Fe replacement deposits had a low-metal concentration or protore but the deposits *sensu stricto* formed subsequently during the Permian, strongly spatially controlled by fault intersections (Fig. 6) (Dill, 1985a). The Fe deposits under study are correlated with those found in the Alpine and extra-Alpine region. The Permian period stood out by a strong subcrustal impact emanating gas and venting basic magma triggered by mantle plumes, which might have played also a significant role in the accumulation of Fe deposits of the current replacement type (Renne et al., 1995; Czamanske et al., 2000; Kamo et al., 2003; Su, 2014).

5.5.4. Replacement deposits related to deep-seated lineamentary fault zones

Three replacement deposits are classified under stage 4: (1) talc replacing dolomite ($Si \Rightarrow CO_2$), (2) halloysite replacing Ca-Mg silicates (Ca-Mg ⇑), (3) calcite replacing quartz/ episyenite ($Ca + CO_2 \Rightarrow Si$). Quantitative leaching of Ca and Mg from Ca-Mg silicates leads to halloysite formation (2) and provides a fluid that is enriched in those elements acting as substitute in talc deposits (1) and episyenite (3). Kaolinization is a prerequisite and predecessor at depth for the structurebound talc and episyenite mineralizations inside as well outside the granites. It provides an alternative source of elements to the Alpine model quoted in Section 5.4.4, which involves basinal Permo-Mesozoic brines that can be ruled out for paleogeographic reasons because the coast line of the Permian sea lies N of the area under study (Szurlies, 2013). The episyenites are younger than the older granite G 1, which yielded a Rb/Sr whole-rock age of 319 ± 3 Ma (Lenz, 1986). The U mineralization at Grossschloppen poses some problems as to formation age of the primary U black ore minerals. Notwithstanding these caveats, an age has been reported showing the upper intercept in the discordia plot at 268 + 51/−48 Ma (Carl and Dill, 1985).

5.5.5. Vein-type and stockwork deposits related to deep-seated lineamentary fault zones

For the Ni-Co- and Pb-Cu-Zn-F mineral associations, no independent age data is recorded. According to the numerous studies in the past, it is a rejuvenation which may cover the interval from the early Mesozoic through the Cenozoic (Dill, 1982, Behr et al., 1987a,b). The fluorite-barite vein-type deposits are of much wider occurrence than the aforementioned ones. Excluding the stockwork-like and disseminated Ni-Co mineral association, all stage 5 – mineral associations are bound to NW-SE-striking structures. They are Permian through Neogene in age, a period during which reactivation of the pre-existing structures such as the Franconian Line was at full swing in the uplifted basement blocks of the Central European Variscides (Dolníček and Slobodník, 2001; Dill et al., 2008b; Wolff et al., 2016)

6. Conclusions

Among the five stages reflecting the evolution of carbonate-hosted and –related mineralization, vein-type, thrustbound and stratabound deposits formed from hydrothermal fluids derived from subcrustal or deep crustal sources. Only the collision-related Sn-W skarn deposits in the Central European Variscides are, based on REE and stable isotope data, without any doubt genetically related to the adjacent, highly fractionated members of the calc-alkaline intrusive rocks. Pegmatite skarn mineralization reveals a strong subcrustal component and a moderate crustal derivation in their mineralizing fluids (Tables 1 and 4).

The Franconian Line was active over a rather long period and was operative already from the waning stages of the Variscan deformation through the Neogene. This is valid for ore (Au, As, Bi, Li, Nb/Ta, Be, U, Fe, Sb, Hg, Mo) and industrial mineral (talc, kaolinite-group minerals, fluorite, barite) assemblages. For the rare Ni-Co and base metal associations, a similar age of formation is assumed for minero-stratigraphic reasons, but cannot be proven with certainty.

Calcsilicate minerals (wollastonite, diopside s.s.s., vesuvianite, grossularite-andradite, clinozoisite-epidote, tremolite-actinolite, prehnite, laumontite, stilbite-heulandite) and carbonate minerals (calcite, dolomite, siderite, Mn siderite, ankerite, rhodochrosite, strontianite, magnesite) constrain the physical-chemical regime over the entire temperature range from 745 °C down to 53 °C and from medium to low pressure at strongly varying redox conditions (Tables 1 and 4) (Hölting and Coldewey, 2013; Röckel, 2014).

Bulk chemical composition, using major and minor elements, the REE variation and Ce and Eu anomalies as well as carbon and oxygen isotopes of the various mineralizations enable us to identify the fluid sources and depict the concentration processes, e.g., mixing of fluids, connate fluid and meteoric fluid interaction (Table 1, Figs. 1, 6–8, 10).

Only for stage 4, including talc, halloysite and U-bearing episyenite, a source-host rock relation can be established. Acidic hydrothermal solution affecting Ca-Mg-Fe silicates of metabasic rocks yielded kaolinization at site and lead to the release of Ca-Mg-bearing fluids required for the built-up of Mg-enriched talc deposits and calcite-bearing uraniferous episyenite.

From an economic point of view, the mineralizing systems which have been derived from subcrustal and deep crustal hydrothermal fluid systems are most prospective for rare element pegmatite, talc, kaolinite-group minerals, iron and uranium. Fluorite and barite are subeconomic in the mineral assemblages inside as well as outside the granites, while base metals and precious metals are only of mineralogical interest. The last mentioned metals predominantly got enriched during the siliceous thrustbound pre-stages and were subjected during the modern stages only to some kind of rejuvenation of their early mineral association by deeply circulating fluids, also accountable for the carbonate-bearing gangue minerals.

Acknowledgements

We express our gratitude to Z. Berner, G. Preuss, C. Mößner and T. Neumann for their technical support concerning REE and C-O isotope determination (Karlsruhe Institute of Technology, Institute for Applied Geosciences, Karlsruhe, Germany). We thank very much three anonymous reviewers for their helpful comments made on our manuscript and we also extend our gratitude to Franco Pirajno, editor-in-chief of ORE GEOLOGY REVIEWS for his editorial handling of our paper.

References

Ackerman, L., Zachariáš, J., Pudilová, M., 2007. P-T and fluid evolution of barren and lithium pegmatites from Vlastějovice, Bohemian Massif, Czech Republic. Int. J. Earth Sci. 96, 623–638.

Ahmed-Said, Y., Leake, B.E., 1996. The conditions of metamorphism of a grossular wollastonite-vesuvianite skarn from the Omey Granite Connemara, western Ireland, with special reference to the chemistry of vesuvianite. Mineral. Mag. 60, 541–550.

Anderson, D.L., Mogk, D.W., Childs, J.F., 1990. Petrogenesis and timing of talc formation in the Ruby Range, southwestern Montana. Econ. Geol. 85, 585–600.

Aral, H., 1989. Antimony mineralization in the northern Murat Dagi (western Turkey). Econ. Geol. 84, 780–787.

Bau, M., 1991. Rare-earth element mobility during hydrothermal and metamorphic fluid-rock interaction and the significance of the oxidation state of europium. Chem. Geol. 93, 219–230.
Bau, M., Möller, P., 1992. Rare earth element fractionation in metamorphogenic hydrothermal calcite, magnesite and siderite. Mineral. Petrol. 45, 231–246.
Bechtel, A., Shieh, Y.-N., Pervaz, M., Püttmann, W., 1996. Biodegradation of hydrocarbons and biogeochemical sulfur cycling in the salt dome environment. Inferences from sulfur isotope and organic geochemical investigations of the Bahloul Formation at the Bou Grine Zn/Pb ore deposit, Tunisia. Geochimica Cosmochimica Acta 60, 2833–2855.
Behr, H.J., Horn, E.E., Frenzel-Beyme, K., Reutel, C., 1987. Fluid inclusion characteristics of the Variscan and post-Variscan mineralizing fluids in the Federal Republic of Germany. Chem. Geol. 61, 273–285.
Behr, H.J., Horn, E.E., Reutel, C., 1987b. Krustenfluide. KTB Ergebnisse der Vorerkundungsarbeiten Lokation Oberpfalz, 2. KTB-Kolloquium Seeheim/Odenwald, 19th–21st September, 1986, pp. 53–61.
Beran, A., 1979. Die Mineralogie von Ankeriten und Sideriten des Steierischen Erzberges und der Radmer. Verhandlungen der Geologischen Bundesanstalt 3, 237–239.
Besang, C., Harre, W., Kreuzer, H., Lenz, H., Müller, P., Wendt, I., 1976. Radiometrische Datierung, geochemische und petrographische Untersuchungen der Fichtelgebirgsgranite. Geologisches Jahrbuch E 8, 3–71.
Bond, D.P.G., Wignall, P.B., 2014. Large Igneous Provinces and Mass Extinctions: An Update. Geological Society of America Special Papers 505. Geological Society of America, Boulder, CO SPE505-02.
Borges, R.M.K., Villas, R.N.N., Fuzikawa, K., Dall'Agnol, R., Pimenta, M.A., 2009. Phase separation, fluid mixing, and origin of the greisens and Potassic episyenite associated with the Água Boa pluton, Pitingatin province, Amazonian craton, Brazil. J. South Am. Earth Sci. 27, 161–183.
Brady, J.B., Cheney, J.T., Rhodes, A.L., Vasquez, A., Green, C., Duvall, M., Kogut, A., Kaufman, L., Kovaric, D., 1998. Isotope geochemistry of Proterozoic talc occurrences in Archaean marbles of the Ruby Mountains, southwest Montana, U.S.A. Geol. Mater. Res. 1, 1–41.
Bucher, K., Grapes, R., 2011. Petrogenesis of Metamorphic Rocks. Springer, Heidelberg, Dortrecht, London, New York, pp. 428.
Budzinski, H., Tischendorf, G., 1985. Modeling of fractional crystallization and granitic magmas: the Variscan postkinematic older granites of Western Erzgebirge– Vogtland, G.D.R. Gerlands Beiträge Geophysik 94, 370–380.
Buschendorf, F., 1930. Die primären Golderze des Hauptganges bei Brandholz im Fichtelgebirge unter besonderer Berücksichtigung ihrer Paragenesis und Genesis. Neues Jahrbuch Mineralogie 62, 1–50.
Carl, C., Dill, H.G., 1985. Age of secondary uranium mineralization in the basement rocks of northeastern Bavaria, F.R.G. Chem. Geol. 52, 295–316.
Castorina, F., Masi, U., 2008. REE and Nd-isotope evidence for the origin of siderite from the Jebel Awam deposit (Central Morocco). Ore Geol. Rev. 34, 337–342.
Černý, P., Ercit, S., Vanstone, P., 1996. Petrology and Mineralization of the Tanco Rare-Element Pegmatite, Southeastern Manitoba. Winnipeg '96. GAC-MAC Fieldtrip Guidebooks.
Chacko, T., 1990. Oxygen isotope geothermometry: the application of a new calibration to granulites (extended abstract). In: Barton, J.M. (Ed.), The Limpopo Belt A field Workshop on Granulites and Deep Crustal Tectonics. Afrikaans University, Johannesburg, pp. 26–31.
Churchman, G.J., Pontifex, I.R., McClure, S.G., 2010. Factors influencing the formation and characteristics of halloysites or kaolinites in granitic and tuffaceous saprolites in Hong Kong. Clays Clay Miner. 58, 220–237.
Czamanske, G.K., Wooden, J.L., Walker, R.J., Fedorenko, A., Siminov, O.N., Budahn, J.R., Siems, D.F., 2000. Geochemical, isotopic, and SHRIMP age data for Precambrian basement rocks, Permian volcanic rocks, and sedimentary host rocks to the ore-bearing intrusions, Noril'sk-Talnakh district, Siberian Russia. Int. Geol. Rev. 42, 895–927.
Debruyne, D., Hulsbosch, N., Muchez, P., 2016. Unraveling rare earth element signatures in hydrothermal carbonate minerals using a source–sink system. Ore Geol. Rev. 72, 232–252.
De Putter, T.D., Andre, L., Bernard, A., Dupuis, C., Jedwab, J., Nicaise, D., Perruchot, A., 2002. Trace element (Th, U, Pb, REE) behavior in a cryptokarstic halloysite and kaolinite deposit from Southern Belgium: importance of "accessory" mineral formation for radioactive pollutant trapping. Appl. Geochem. 17, 1313–1328.
Derry, L.A., Brasier, M.D., Corfield, R.M., Rozanov, A.Yu., Zhuravlev, A.Yu., 1994. Sr and C isotopes in Lower Cambrian carbonates from the Siberian Craton: a paleoenvironmental record during the 'Cambrian explosion'. Earth Planetary Sci. Lett. 128, 678–681.
Dill, H.G., 1982. Kobaltminerale aus den Nailaer Eisenspatgängen. Z. Dtsch. Geol. Ges. 133, 643–647.
Dill, H.G., 1983. Plutonic mobilization, sodium metasomatism, propylitic, wall rock alteration and element partitioning from Höhensteinweg uranium occurrence (Northeast Bavaria). Uranium 1, 139–166.
Dill, H.G., 1985a. Die Vererzung am Westrand der Böhmischen Masse. – Metallogenese in einer ensialischen Orogenzone. Geologisches Jahrbuch D 73, 3–461.
Dill, H.G., 1985b. Antimoniferous mineralization from the Mid-European Saxothuringian Zone; mineralogy, geology, geochemistry and ensialic origin. Int. J. Earth Sci. 74, 447–466.
Dill, H.G., 1989. Metallogenetic and geodynamic evolution in the Central European Variscides. A pre-well site study for the German Continental Deep Drilling Programme. Ore Geol. Rev. 4, 279–304.
Dill, H.G., 2010. The "chessboard" classification scheme of mineral deposits: mineralogy and geology from aluminum to zirconium. Earth-Sci. Rev. 100, 1–420.
Dill, H.G., 2015a. Pegmatites and aplites: their genetic and applied ore geology. Ore Geol. Rev. 69, 417–561.
Dill, H.G., 2015b. The Hagendorf-Pleystein Province: The center of pegmatites in an ensialic orogen. ISBN-978-3-319-18805-8 In: Modern Approaches in Solid Earth Sciences. Springer, Dortrecht, Heidelberg, London, New York, pp. 475.
Dill, H.G., 2016. Kaolin: soil, rock and ore From the mineral to the magmatic, sedimentary, and metamorphic environments. Earth Sci. Rev. 161, 16–129.
Dill, H.G., Weiser, T., 1981. Eine Molybdän-Sulfid-Impsonit-Mineralisation aus dem Uran-Vorkommen Wäldel/Mähring (Oberpfalz). Neues Jahrbuch für Mineralogie 452–458.
Dill, H.G., Kantor, W., 1997. Depositional environment, chemical facies and a tentative classification of some selected phosphate accumulations. Geologisches Jahrbuch D 105, 3–43.
Dill, H.G., Dulski, P., Möller, P., 1986. Fluorite mineralization and REE patterns in vein-type deposits from the N Bavarian Basement (Germany). Neues Jahrbuch für Mineralogie Abhandlungen 154, 141–151.
Dill, H.G., Sachsenhofer, R.F., Grecula, P., Sasvári, T., Palinkaš, L.A., Borojević-Šoštarić, S., Strmić-Palinkaš, S., Prochaska, W., Garuti, G., Zaccarini, F., Arbouille, D., Schulz, H.-M., 2008a. Fossil fuels, ore – and industrial minerals. In: McCann, T. (Ed.), Geology of Central Europe, Geological Society of London. Special Publication, London, pp. 1341–1449.
Dill, H.G., Melcher, F., Gerdes, A., Weber, B., 2008b. The origin and zoning of hypogene and supergene Fe-Mn-Mg-Sc-U-REE-Zn phosphate mineralization from the newly discovered Trutzhofmühle aplite (Hagendorf pegmatite province, Germany). Can. Mineral. 46, 1131–1157.
Dill, H.G., Botz, R., Berner, Z., Abu Hamad, A.M.B., 2010. The origin of pre – and syn-rift, hypogene Fe-P mineralization during the Cenozoic along the Dead-Sea-Transform Fault, Northwest Jordan. Econ. Geol. 105, 1301–1319.
Dill, H.G., Hansen, B.T., Weber, B., 2011. REE contents, REE minerals and Sm/ Nd isotopes of granite- and unconformity-related fluorite mineralization at the western edge of the Bohemian Massif: with special reference to the Nabburg-Wölsendorf District, SE Germany. Ore Geol. Rev. 40, 132–148.
Dill, H.G., Skoda, R., Weber, B., Müller, A., Berner, Z.A., Wemmer, K., Balaban, S.-I., 2013. Mineralogical and chemical composition of the Hagendorf-North Pegmatite, SE Germany – a monographic study. Neues Jahrbuch für Mineral, Abhandlungen, pp. 281–318.
Dixon, J.B., McKee, T.R., 1974. Internal and external morphology of tubular and spheroidal halloysite particles. Clays Clay Miner. 22, 127–137.
Dolníček, Z., Slobodník, M., 2001. The neoidic fluorite mineralization in the Brno Massif: interaction between fluid and rock. Geolines 13, 51–52.
Dolníček, Z., Rene, M., Hermannova, S., Prochaska, W., 2013. Origin of the Okrouhla Radouň episyenite-hosted uranium deposit, Bohemian Massif, Czech Republic: fluid inclusion and stable isotope constraints. Miner. Deposita 49, 409–425.
Dosbaba, M., Novák, M., 2012. Quartz replacement by "kerolite" in graphic quartz–feldspar intergrowths from the Věžná I pegmatite, Czech Republic: a complex desilication process related to episyenitization. Can. Mineral. 50, 1609–1622.
Dubois, M., Lopez, M., Orberger, B., Rodriguez, C., Boussafir, M., Dreux, G., Rodrigues, S., Pambo, F., 2015. The Mn-carbonate rich black shales of the Bangombe Plateau, Francevillian basin, Gabon. In: André-Mayer, A.S., Cathelineau, M., Muchez, Ph, Pirard, E., Sindern, S. (Eds.), Mineral Resources in a Sustainable World. Proceedings of the 13th Biennial SGA Meeting, pp. 1–4.
Ebner, F., Cerny, I., Eichhorn, R., Götzinger, M.A., Paar, W.H., Prochaska, W., Weber, L., 2000. Mineral resources in the Eastern Alps and adjoining areas. In: Neubauer, F., Höck, V. (Eds.), Aspects of Geology in Austria. Mitteilungen der Österreichischen Geologischen Gesellschaft, pp. 157–184.
Felser, H., Seeliger, E., Strunz, H., 1965. Die Erzmineralparagenese im Marmor von Wunsiedel/Fichtelgebirge. Acta Albertina 26, 35–53.
Finger, F., Roberts, M.P., Haunschmid, B., Schermaier, A., Steyrer, H.P., 1997. Variscan granitoids of central Europe: their typology, potential sources and tectonothermal relations. Min. Petrol. 6, 67–96.
Firstova, A., Stepanova, T., Cherkashov, G., Goncharov, A., Babaeva, S., 2016. Composition and formation of gabbro-peridotite hosted seafloor massive sulfide deposits from the Ashadze-1 hydrothermal field, Mid-Atlantic Ridge. Minerals 6, 1–20.
Franke, W., 1995. Introduction-Saxo-Thuringian Basin. In: Dallmeyer, D., Franke, W., Weber, K. (Eds.), Pre-permian geology of Central and Western Europe. Springer, Berlin, pp. 33–49.
Franke, W., Kreuzer, H., Okrusch, M., Schüssler, U., Seidel, E., 1995. Saxothuringian Basin: Exotic Metamorphic Nappes, Stratigraphy, Structure and Igneous Activity. Pre-Permian geology of Central and Western Europe. Springer, Berlin, pp. 277–294.
Friedrich, G., Kontny, A., Vogtmann, J., 1988. Die Verteilung von Sulfiden, Rutil und Ilmenit in phyllitischen Gesteinen der KTB-Geothermiebohrung Neusorg/Oberpfalz. Geologische Blätter NO-Bayern 38, 169–196.
Friedrich, G., Kontnik, M., Vogtmann-Becker, J., Herzig, P., Kontny, A., Keyssner, J.S., 1989. Sulfidchemismus als Temperaturindikator in den Gesteinen der ZEV. Poster-Abstract 2. KTB-Schwerpunktkolloquium 15, Giesen.
Friedrich, G., Herzig, P., Kontny, A., Vogtmann-Becker, J., Keyssner, S., 1991. Erzpetrologie in der KTB-Vorbohrung. KTB-Report 1986–1990, 136–157.
Gagnon, J.E., Samson, I.M., Fryer, B.J., Williams-Jones, A.E., 2003. Compositional heterogeneity in fluorite and the genesis of fluorite deposits. Insights from LA–ICP–MS analysis. Can. Mineral. 41, 365–382.
Gilbert, J.M., Park Jr., C.F., 2007. The Geology of Ore Deposits. Waveband Press, Long Grove, IL, pp. 985.
Glodny, J., Grauert, B., Krohe, A., 1995. Ordovizische Pegmatite in variszischen HT-Metamorphiten des KTB-Umfeldes: hinweis auf hohe Stabilität des Rb–Sr-Systems in Muskoviten. Terra Nostra 95, 98.
Grasby, S.E., Beauchamp, B., Bond, D.P.G., Wignall, P.B., Sanei, H., 2016. Mercury anomalies associated with three extinction events (Capitanian Crisis, Latest Permian Extinction and the Smithian/Spathian Extinction) in NW Pangea. Geol. Mag. 153,

285–297.
Hecht, L., Freiberger, R., Gilg, H.A., Grundmann, G., Kostitsyn, Y.A., 1999a. Rare earth element and isotope (C, O, Sr) characteristics of hydrothermal carbonates: genetic implications for dolomite-hosted talc mineralization at Göpfersgrün (Fichtelgebirge, Germany). Chem. Geol. 155, 115–130.
Hecht, L., Thuro, K., Plinninger, R., Cuney, M., 1999b. Mineralogical and geochemical characteristics of hydrothermal alteration and episyenitiztion in the Königshain granites, northern Bohemian massif, Germany. Int. J. Earth Sci. 88, 236–252.
Hoefs, J., 2015. Stable Isotope Geochemistry. Springer, Heidelberg, pp. 359.
Hölting, B., Coldewey, W.G., 2013. Hydrogeologie. Einführung in die Allgemeine und Angewandte Hydrogeologie, 8 Edition. Springer-Verlag, Berlin, Heidelberg, pp. 392.
Huang, X.-W., Qi, L., Meng, Y.-M., Chen, D., Ling, H.-D., 2015. Origin of siderite mineralization in western Guizhou, SW China: constraints from REEs, C., O, Sr and S isotopes. Ore Geol. Rev. 66, 252–265.
Irber, W., Möller, P., Bach, W., 1998. Leaching experiments with acid cation-exchange resin as a new tool to estimate element availabilities in geological samples. Water rock interaction, Balkema, Rotterdam, pp. 839–842.
Jenkin, G.R.T., Lusty, P.A.J., McDonald, I., Smith, M.P., Boyce, A.J., Wilkinson, J.J., 2015. Ore deposits in an evolving earth geological society. Special Publication 393, 1–333.
Joussein, E., Petit, S., Churchman, J., Theng, B., Righi, D., Delvaux, B., 2005. Halloysite clay minerals – a review. Clay Miner. 40, 383–426.
Jung, R., Hoell, R., 1982. Wolframvorkommen in Nordost-Bayern. Erzmetall 35, 142–147.
Kamo, S.L., Czamanske, G.K., Amelin, Y., Fedorenko, A., Davis, D.W., Trofimov, R., 2003. Rapid eruption of Siberian flood-volcanic rocks and evidence for coincidence with the Permian-Triassic boundary.Earth. Planetary Sci. Lett. 214, 75–91.
Klinkhammer, G.P., Elderfield, H., Hudson, A., 1983. Rare earth elements in seawater near hydrothermal vents. Nature 305, 185–188.
Kolb, J., Kisters, A.F.M., Hoernes, S., Meyer, F.M., 2000. The origin of fluids and nature of fluid-rock interaction in auriferous mylonites of the Renco Mine, southern Zimbabwe. Miner. Deposita 35, 109–125.
Kouchinsky, A., Bengtson, S., Gallet, Y., Korovnikov, I.V., Pavlov, V.E., Runnegar, B., Shields-Zhou, G.A., Veizer, J., Young, E.D., Ziegler, K., 2008. The SPICE carbon isotope excursion in Siberia: a combined study of the upper Middle Cambrian lowermost Ordovician Kulyumbe River section, northwestern Siberian Platform. Geol. Mag. 145, 609–622.
Kreuzer, H., Seidel, E., Schüssler, U., Okrusch, M., Lenz, K.-L., Raschka, H., 1989. K-Ar geochronology of different tectonic units of the northwestern margin of the Bohemian Massif. Tectonophysics 157, 149–178.
Krolop, P., Burisch, M., Richter, L., Fritzke, B., Seifert, T., 2018. Antimoniferous vein-type mineralization of the Berga Antiform, Eastern-Thuringia, Germany: a fluid inclusion study. Chem. Geol. (on-line. https://doi.org/10.1016/j.chemgeo.2018.02.034).
Kroner, U., Hahn, T., 2004. Sedimentation, Deformation und Metamorphose im Saxothuringikum während der variszischen Orogenese: Die komplexe Entwicklung von Nord. Gondwana während kontinentaler Subduktion und schiefer Kollision. In: Linnemann, U. (Ed.), Das Saxothurigikum, Geologica Saxonia 48/49. Dresden, Staatliche Naturhistorische Sammlungen, pp. 133–146.
Krupp, R.E., 1988. Solubility of stibnite in hydrogen sulfide solutions, speciation and equilibrium constants from 25°C to 350°C. Geochim. Cosmochim. Acta 52, 3005–3015.
Krylov, D.P., 1985. Model temperatures estimated using oxygen isotopic distribution. Doklady Acad Nauk SSSR (Trans USSR Acad Sci) 285, 1201–1204.
Leighton, M.W., Pendexter, C., 1962. Carbonate rock types. In: Ham, W.E. (Ed.), Classification of Carbonate Rocks. Amer. Assoc. Petrol. Geol. Mem., pp. 62–85.
Lenz, H., 1986. Rb/Sr-Gesamtgesteins-Altersbestimmung am Weißenstadt-Marktleuthener porphyrgranite des fichtelgebirges. Geologisches Jahrbuch E 34, 67–76.
Leroy, J., 1978. Metallogenèse de gisements úranium de la division de la Crouzille. Ph.D. thesis. University Nancy, pp. 276..
Linnemann, U., 2003. Die Struktureinheiten des Saxothurigikums. In: Linnemann, U. (Ed.), Das Saxothuringikum, Gelogica Saxonica 48/49. Staatliche Naturhistorische Sammlungen, Dresden, pp. 19–28.
López-Moro, F.J., Moro, M.C., Timón, S.M., Cembranos, M.L., Cóar, J., 2013. Constraints regarding gold deposition in episyenites: the Permian episyenites associated with the Villalcampo shear zone, central western Spain. Int. J. Earth Sci. 102, 721–744.
Möller, P., Giese, U., 1997. Determination of easily accessible metal fractions in rocks by batch leaching with acid cation-exchange resin. Chem. Geol. 137, 41–55.
Munoz, M., Courjault-Rade, P., Tollon, F., 1992. The massive stibnite veins of the French Palaeozoic basement: a metallogenic marker of Late Variscan brittle extension. Terra Nova 4, 171–177.
Novák, M., Hyršl, J., 1992. Locality No. 3: Vlastějovice near Zruč nad Sázavou, pegmatites with fluorite penetrating skarn. In: Novák, M., Černý, P. (Eds.), International symposium on mineralogy, petrology and geochemistry of granitic pegmatites Lepidolite 200. Czech Republic. Field trip guidebook, Nové Město na Moravě, pp. 33–37.
Patel, S.C.J., 2007. Vesuvianite-wollastonite-grossular-bearing calc-silicate rock near Tatapani, Surguja district, Chhattisgarh. J. Earth Syst. Sci. 116, 143–147.
Partington, G.A., McNaughton, N.J., Williams, I.S., 1995. A review of the geology, mineralization, and geochronology of the greenbushes pegmatite, Western Australia. Econ. Geol. 90, 616–635.
Petersson, J., Eliasson, T., 1997. Mineral evolution and element mobility during episynitization (dequartzification) and albitization in the post-kinematic Bohus Granite, southwest Sweden. Lithos 42, 123–146.
Recio, C., Fallick, A.E., Ugidos, J.M., Stephens, W.E., 1997. Characterization of multiple fluid-granite interaction processes in the episyneites of Avila-Béjar, central Iberian massif, Spain. Chem. Geol. 143, 127–144.
Ren, Y., Zhong, D., Gao, C., Yang, Q., Xie, R., Jia, L., Jiang, Y., Zhong, N., 2017. Dolomite geochemistry of the Cambrian Longwangmiao Formation, eastern Sichuan Basin: implication for dolomitization and reservoir prediction. Petroleum Res. 2, 64–76.
Renne, P.R., Zichao, Z., Richards, M.A., Black, M.T., Basu, A.R., 1995. Synchrony and causal relations between Permian-Triassic boundary crises and Siberian flood volcanism. Science 269, 1413–1416.
Reutel, C., 1992. Krustenfluide in Gesteinen und Lagerstätten am Westrand der Böhmischen Masse. Göttinger Arbeiten zur Geologie und Paläontologie 53, 1–75.
Reutel, C., Horne, E.E., Topp, J., 1989. Paläofluiduntersuchungen am Bohrprofil der KTB-Vorbohrung – Vergleich zum Umfeld in Emmermann. KTB Report 89-3. KTB Meeting, pp. 454.
Richter, P., Stettner, G., 1979. Geochemische und petrographische Untersuchungen der Fichtelgebirgsgranite. Geologica Bavarica 78, 1–144.
Richter, P., Okrusch, M., Bohlender, F., 1988. Die geothermie-bohrung neusorg im Fichtelgebirge: petrographie und geochemie des kernmaterials. Geologische Blätter NO-Bayern 38, 125–168.
Ridley, J., 2013. Ore Deposit Geology. Cambridge University Press, pp. 409 pp..
Röckel, L., 2014. Hydrogeothermale Charakterisierung der Bohrung Weißenstadt. B.Sc Thesis. Karlsruhe Institut für Technologie, pp. 95.
Rumble III, D., 1982. Stable isotope fractionation during metamorphic volatilization reactions. In: J.M. F (Ed.), Characterization of metamorphism through mineral equilibria. Reviews in Mineralogy, pp. 153–206.
Sánchez, V., Cardellach, E., Corbella, M., Vindel, E., Martín-Crespo, T., Boyce, A.J., 2010. Variability in fluid sources in the fluorite deposits from Asturias (N Spain): further evidences from REE, radiogenic (Sr, Sm, Nd) and stable (S, C, O) isotope data. Ore Geol. Rev. 37, 87–100.
Schneiderhöhn, H., 1961. Die Pegmatite [The pegmatites]. Gustav Fischer Verlag, Stuttgart, pp. 720 (in German).
Selway, J.B., Černy, P., Hawthorne, F.C., Novák, M., 2000. The Tanco pegmatite at Bernic Lake, Manitoba. 15. Internal tourmaline. Can. Mineral. 38, 877–891.
Shoji, T., 1975. Role of temperature and CO_2 pressure in the formation of skarn and its bearing on mineralization. Econ. Geol. 70, 739–749.
Song, G., Qin, K., Li, G., Evans, N.J., Chen, L., 2014. Scheelite elemental and isotopic signatures: implications for the genesis of skarn-type W-Mo deposits in the Chizhou Area, Anhui Province, Eastern China. Am. Mineral. 99, 303–317.
Stettner, G., 1959. Die Lagerstätte des Specksteins von Göpfersgrün-Thiersheim im Fichtelgebirge. Geologica Bavarica 42, 1–72.
Su, B.-X., 2014. Permian Mantle Plume and Paleozoic Tectonic Evolution. Mafic-ultramafic Intrusions in Beishan and Eastern Tianshan at Southern CAOB: Petrogenesis, Mineralization and Tectonic Implication. Springer Theses Springer, Berlin, Heidelberg.
Szurlies, M., 2013. Late Permian (Zechstein) magnetostratigraphy in Western and Central Europe Geological Society. London, Special Publications 376, 73–85.
Teuscher, E.O., Weinelt, W., 1972. Die metallogenese im raum spessart-fichtelgebirge-oberpfälzer wald- bayerischer wald. Geologica Bavarica 65, 5–73.
Timon Sanchez, S.M., Moro Benito, M.C., Cembranos Pérez, M.L., 2009. Mineralogical and physiochemical evolution of the Los Santos scheelite skarn, Salamanca, NW Spain. Econ. Geol. 104, 961–965.
Valley, J.W., 1986. Stable isotope geochemistry of metamorphic rocks. In: Valley, J.W., Taylor, H.P., O'Neil, J.R. (Eds.), Stable isotopes in high temperature geological processes. Reviews in Mineralogy, pp. 445–490.
Van Lichtervelde, M., Linnen, R.L., Salvi, S., Beziat, D., 2006. The role of metagabbro rafts on tantalum mineralization in the Tanco granitic pegmatite, Manitoba. Can. Mineral. 44, 625–644.
Von Horstig, G., Teuscher, E.O., 1979. Die Eisenerze im Alten Gebirge NE-Bayerns. Geologisches Jahrbuch D 31, 7–47.
Weaver, C.E., 1989. Clays, Muds, and Shales. Elsevier, Amsterdam, pp. 819.
Wemmer, K., Ahrendt, H., 1993. Age determination on retrograde processes in rocks of the KTB and the surrounding area. KTB-Report 93–2, 129–131.
Wiegand, B., Hansen, B.T., Becker, T., 1994. Time of Sr-isotope homogenization in marbles and calcsilicate rocks of the Saxothuringian-Moldanubian transition zone. Zentralblatt für Geologie und Paläontologie. 1994,5/6 (1994): Tenth Meeting on Geodynamics of the European Variscides. First Symposium on Permocarboniferous Igneous Rocks, Bayreuth, pp. 469–472.
Winchester, J.A., 2002. Pace Tmr network Team, Palaeozoic amalgamation of Central Europe: new results from recent geological and geophysical investigations. Tectonophysics 360, 5–21.
Winkler, H.G.F., 1976. Petrogenesis of Metamorphic Rocks. Springer, New York, pp. 348.
Wolff, R., Dunkl, I., Kempe, U., Stockli, D., Wiedenbeck, M., von Eynatten, H., 2016. Variable helium diffusion characteristics in fluorite. Geochim. Cosmochim. Acta 188, 21–34.
Wurm, A., 1932. Erläuterungen zur Geologischen Karte von Bayern 1: 25 000, Blatt Wunsiedel Nr. 82. Bayerisches Oberbergamt, München, pp. 46.
Wurm, A., 1961. Geologie von Bayern. Gebrüder Bornträger, Berlin, pp. 555.
Žáček, V., Novák, M., Raimboult, L., Zachariáš, J., Ackerman, L., 2003. Locality No. 8: Vlastějovice near Ledeč nad Sázavou. Fe-skarn, barren fluorite pegmatite. In: Novák, M. (Ed.), International symposium on light elements in rock forming minerals LERM 2003. Czech Republic. Field trip guidebook, Nové Město na Moravě, pp. 61–70.
Zulauf, G., 1990. Spät- bis postvarsizische Deformation und Spannungsfelder in der nördlichen Oberpfalz (Bayern) unter besonderer Berücksichtigung der KTB Vorbohrung. Frankfurter Geowissenschaftliche Arbeiten Series A 8, 1–285.